The Plant Cell, Vol. 29: 508–525, March 2017, www.plantcell.org 

# Sumoylation of *Turnip mosaic virus* RNA Polymerase Promotes Viral Infection by Counteracting the Host NPR1-Mediated Immune Response

**Xiaofei Cheng,[a,1] Ruyi Xiong,[a,b,1,2] Yinzi Li,[a,b] Fangfang Li,[a] Xueping Zhou,[c] and Aiming Wang[a,b,3]**

[a] London Research and Development Centre, Agriculture and Agri-Food Canada, London, Ontario N5V 4T3, Canada
[b] Department of Biology, Western University, London, Ontario N6A 5B7, Canada
[c] State Key Laboratory of Rice Biology, Zhejiang University, Hangzhou, Zhejiang 310058, China

**Sumoylation is a transient, reversible dynamic posttranslational modification that regulates diverse cellular processes including plant-pathogen interactions. Sumoylation of NPR1, a master regulator of basal and systemic acquired resistance to a broad spectrum of plant pathogens, activates the defense response. Here, we report that NIb, the only RNA-dependent RNA polymerase of *Turnip mosaic virus* (TuMV) that targets the nucleus upon translation, interacts exclusively with and is sumoylated by SUMO3 (SMALL UBIQUITIN-LIKE MODIFIER3), but not the three other *Arabidopsis thaliana* SUMO paralogs. TuMV infection upregulates SUMO3 expression, and the sumoylation of NIb by SUMO3 regulates the nuclear-cytoplasmic partitioning of NIb. We identified the SUMO-interacting motif in NIb that is essential for its sumoylation and found that knockout or overexpression of SUMO3 suppresses TuMV replication and attenuates viral symptoms, suggesting that SUMO3 plays dual roles as a host factor of TuMV and as an antiviral defender. Sumoylation of NIb by SUMO3 is crucial for its role in suppressing the host immune response. Taken together, our findings reveal that sumoylation of NIb promotes TuMV infection by retargeting NIb from the nucleus to the cytoplasm where viral replication takes place and by suppressing host antiviral responses through counteracting the TuMV infection-induced, SUMO3-activated, NPR1-mediated resistance pathway.**

## INTRODUCTION

Posttranslational modifications (PTMs) play crucial roles in diverse biological processes including plant-pathogen interactions. In addition to phosphorylation, glycosylation, and ubiquitination, sumoylation has emerged as a key PTM that plays a role in diversifying proteasome activity (Geiss-Friedlander and Melchior, 2007). Sumoylation is a transient, highly dynamic process by which small ubiquitin-like modifiers (SUMOs), a group of ubiquitin-related modifiers ~100 amino acids in length, are covalently conjugated to cellular target proteins. SUMOs may also interact with the SUMO-interaction motifs (SIMs) of some target substrates noncovalently (Kerscher, 2007). The number of SUMO genes varies in different eukaryote genomes. For example, budding yeast (*Saccharomyces cerevisiae*), flies (*Drosophila melanogaster*), and worms (*Caenorhabditis elegans*) have only a single SUMO gene, whereas vertebrates have up to four paralogs (Geiss-Friedlander and Melchior, 2007) and the model plant *Arabidopsis thaliana* has eight SUMO paralogs (Kurepa et al., 2003; Novatchkova et al., 2004). Despite this variation, sumoylation is highly conserved among yeast, vertebrates, and plants and is performed through a multistep enzymatic reaction (Kerscher et al., 2006; Dye and Schulman, 2007). First, SUMO precursors are proteolytically processed to expose their C-terminal double glycine (Gly-Gly) motifs by SUMO-specific proteases (also referred to as ubiquitin-like proteases). Subsequently, the mature form of SUMO is transferred to the SUMO-activating E1 enzyme (SAE1/SAE2 in Arabidopsis; AOS1/UBA2 in yeast and mammals) and further to the SUMO-conjugating E2 enzyme (SCE1 in plants or Ubc9 in yeast and mammals). Finally, in a process catalyzed by SUMO E3 ligase, SUMO from the SUMO-E2 conjugate is transferred and conjugated to target proteins via isopeptide bond formed between the C-terminal Gly-Gly motif of SUMO and the lysine residue within the conserved sumoylation motif (ψ-K-X-E/D) in the target protein (where ψ represents a hydrophobic amino acid residue, including Leu, Ile, Val, or Phe) (Melchior, 2000; Bernier-Villamor et al., 2002). Sumoylation is reversible; the reverse process, termed deconjugation or desumoylation, is also catalyzed by the SUMO-specific protease (Colby et al., 2006).

PTMs have been implicated in viral infection (Wang, 2015; Nagy, 2016). For example, phosphorylation of *Cucumber mosaic virus*-encoded 2a protein (RNA-dependent RNA polymerase [RdRp]) prevents its interaction with the viral 1a protein to inhibit viral replication (Kim et al., 2002). The 66K RdRp of *Turnip yellow mosaic virus* is phosphorylated and ubiquitinated, which facilitates the degradation of the 66K protein and inhibits viral replication (Jakubiec et al., 2007; Camborde et al., 2010). The degradation of 66K can be counteracted by the interaction with viral 98K replicase, a deubiquitinating enzyme (Chenon et al., 2012). Over the past several years, an increasing body of evidence

[1] These authors contributed equally to this work.
[2] Current address: Department of Biology, University of Saskatchewan, 112 Science Place, Saskatoon, Saskatchewan S7N 5E2, Canada.
[3] Address correspondence to aiming.wang@agr.gc.ca.
The author responsible for distribution of materials integral to the findings presented in this article in accordance with the policy described in the Instructions for Authors (www.plantcell.org) is: Aiming Wang (aiming.wang@agr.gc.ca).
www.plantcell.org/cgi/doi/10.1105/tpc.16.00774

has shown that sumoylation also affects viral infection (Wimmer et al., 2012; Everett et al., 2013; Varadaraj et al., 2014; Sloan et al., 2015). The M1 and NS1 proteins of Influenza A virus, the gag protein of *Human immunodeficiency virus*, and the nonstructural protein 5 (NS5) of *Dengue virus* (DENV) are sumoylated during viral infection (Gurer et al., 2005; Wu et al., 2011; Xu et al., 2011; Gao et al., 2015; Su et al., 2016). Sumoylation of the RdRp 3D protein of *Enterovirus 71* (EV71) facilitates viral replication, likely via stabilization of the 3D protein (Liu et al., 2016b). The replication protein (also referred to as AL1, Rep, or AC1) of *Tomato golden mosaic virus*, a plant geminivirus, interacts with SCE1; such an interaction is crucial for *Tomato golden mosaic virus* infection (Castillo et al., 2004; Sánchez-Durán et al., 2011). However, the exact role of sumoylation in viral infection is still far from being fully understood.

Potyviruses represent the largest family of known plant viruses, including many agriculturally important viruses such as *Turnip mosaic virus* (TuMV), *Plum pox virus*, *Soybean mosaic virus*, *Potato virus A*, and *Tobacco etch virus* (Revers and García, 2015). The genome of TuMV is a single-stranded RNA of ~9.6 kb that has a viral protein genome-linked (VPg) covalently linked to its 5′ end and a poly(A) tail at the 3′ end. The viral genome contains a single open reading frame encoding a large polypeptide of ~350 kD that is ultimately cleaved into 10 mature proteins (Urcuqui-Inchima et al., 2001). In addition, transcriptional slippage on the P3 cistron enables expression of an additional protein, P3N-PIPO (Chung et al., 2008; Olspert et al., 2015; Rodamilans et al., 2015), which is indispensable for cell-to-cell movement by potyviruses (Wei et al., 2010b; Wen and Hajimorad, 2010). Of these 11 mature viral proteins, NIb is the only one that contains the conserved GDD motif of RdRp (Koonin, 1991). We recently reported that NIb interacts with SCE1 and that this interaction is essential for potyviral infection (Xiong and Wang, 2013). It is well known that the potyviral NIb is a nuclear targeting protein (Restrepo et al., 1990). However, the functional role of NIb targeting to the nucleus remains a mystery.

In this study, we demonstrate that the nucleus-located TuMV NIb selectively interacts with SUMO3 for sumoylation and that sumoylation of NIb by SUMO3 counteracts the TuMV infection-induced, SUMO3-activated NONEXPRESSER OF PATHOGENESIS-RELATED GENES1 (NPR1)-mediated resistance pathway. Moreover, the sumoylated form of NIb retargets the cytoplasm where the replication complex resides. This study reveals the molecular mechanism by which sumoylation of NIb by SUMO3 facilitates TuMV infection.

## RESULTS

### TuMV Infection Upregulates SUMO3 Expression

In a recent study, we found the NIb protein of TuMV interacts with SCE1, the only SUMO conjugation enzyme of Arabidopsis, and that knockdown of SCE1 inhibits viral infection (Xiong and Wang, 2013). Of the eight SUMO genes in Arabidopsis, only four, namely, SUMO1, SUMO2, SUMO3, and SUMO5, are known to be functional (Saracco et al., 2007; Budhiraja et al., 2009). Among these four SUMO paralogs, SUMO1 and SUMO2 are closely related, sharing 87.9% amino acid sequence identity, whereas SUMO3 and SUMO5 only share 47.0% and 35.7% amino acid sequence identity with SUMO1, respectively. Multiple sequence alignment and phylogenetic analysis revealed that none of the four Arabidopsis SUMO paralogs is clustered with human SUMO paralogs, suggesting the independent expansion of mammal and plant SUMO genes (Supplemental Figure 1 and Supplemental File 1; Colby et al., 2006). Published data also indicate that SUMO1 and SUMO2 are ubiquitously expressed and that the expression of SUMO3 and SUMO5 appears to be highly tissue specific (Saracco et al., 2007; van den Burg et al., 2010). SUMO1 and SUMO2 apparently play a predominant, redundant role in endogenous protein sumoylation, as single mutants of SUMO1 and SUMO2 paralogs do not exhibit distinguishable phenotypes and the double-null mutant is embryo lethal (Castaño-Miquel et al., 2011). Since the expression and subcellular localization of SUMO5 had not yet been experimentally examined, we analyzed the expression patterns and subcellular localization of these four Arabidopsis SUMO paralogs. The SUMO transcripts were evaluated by qRT-PCR in five different tissues, namely, root, stem, leaf, flower, and seed tissue. We found that SUMO1 and SUMO2 were highly expressed in all tissues, and SUMO3 transcripts were abundantly present in stems and seeds and, to a much lesser extent, in root, leaf, and flower tissues (Figure 1A). Interestingly, SUMO5 was predominantly expressed in flower tissue, suggesting a potential role for SUMO5 in flowering or embryo development (Figure 1A). These results are largely consistent with the expression profiles obtained through analysis of the DNA microarray expression data and GUS assays (Saracco et al., 2007; van den Burg et al., 2010).

To study the subcellular localization patterns of the Arabidopsis SUMO paralogs, we cloned the coding regions of the SUMO genes and fused them to the C terminus of YFP, which prevents the release of YFP from the C terminus by endogenous SUMO proteases. The chimeric genes were transiently expressed in *Nicotiana benthamiana* leaves through agroinfiltration and monitored by confocal microscopy. Consistent with a previous report (Lois et al., 2003), YFP signals were observed in both the nucleus (excluding the nucleolus) and cytoplasm in cells expressing YFP-SUMO1, YFP-SUMO2, and YFP-SUMO3 (Figure 1B). YFP signals from YFP-SUMO5 were mainly present in the nucleus, and a small portion of the fluorescence (appearing as granules) was also observed in the cytoplasm. Additionally, two distribution patterns were observed in the nuclei of cells expressing YFP-SUMO5: signals in nuclear bodies (in ~70% nuclei) and diffuse signals in both the nucleoplasm and nucleolus (~30% nuclei). Immunoblotting with GFP antibodies revealed multiple bands with various molecular weights, suggesting that N-terminal YFP-tagged SUMO1, SUMO2, SUMO3, and SUMO5 can be processed and conjugated to substrate proteins by the *N. benthamiana* sumoylation pathway (Figure 1C). Thus, the fluorescence of YFP-SUMO1, YFP-SUMO2, YFP-SUMO3, and YFP-SUMO5 represented the unconjugated form of YFP-SUMO fusions and the proteins they modified. Taken together, these results confirm that the four Arabidopsis SUMO paralogs exhibit distinct expression and subcellular localization patterns, implying that they have distinct functions.

SUMO3 is also induced by salicylic acid, an essential signaling molecule in plant defense against pathogens, and by the defense elicitor Flg22, suggesting a possible role for SUMO paralogs in

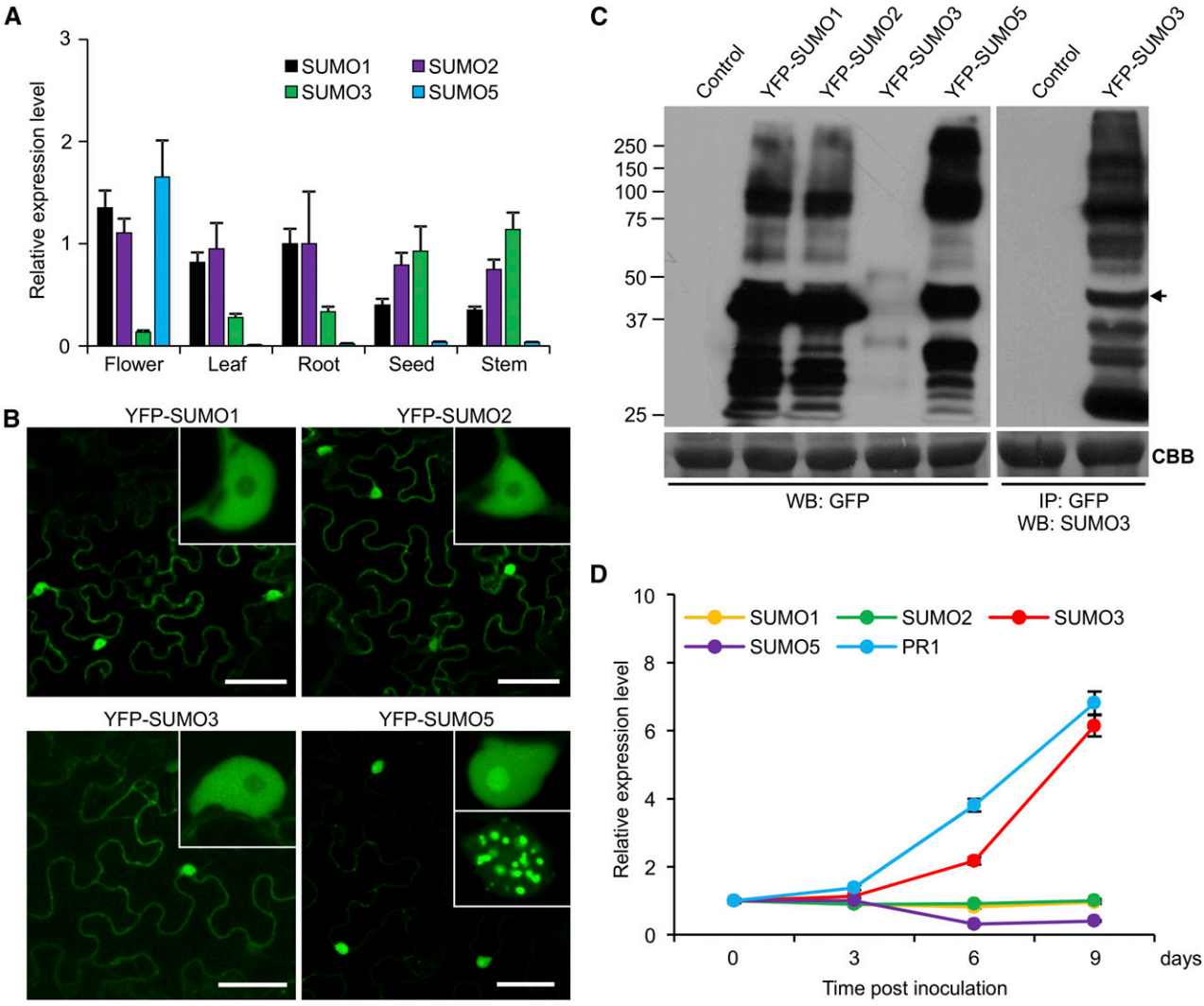


**Figure 1.** TuMV Infection Upregulates SUMO3 Expression.

**(A)** The expression profiles of SUMO1, SUMO2, SUMO3, and SUMO5 in various Arabidopsis organs. The Arabidopsis *ACTIN II* gene was used as the internal control. Bars represent SD from three experiments (each with five technical replicates).

**(B)** Subcellular localization of YFP-SUMO1, YFP-SUMO2, YFP-SUMO3, and YFP-SUMO5 in *N. benthamiana* epidermal cells at 2 dpi. The yellow fluorescence is rendered in green. Bars = 50 μm. Insets show typical nuclear signals.

**(C)** Immunoblotting analyses of transiently expressed YFP-SUMO1, YFP-SUMO2, YFP-SUMO3, and YFP-SUMO5. Note that due to the low expression of YFP-SUMO3, the affinity purification was performed with anti-GFP Sepharose and detected with SUMO3 antibodies. Arrowhead indicates the size of monomers YFP-SUMO1, YFP-SUMO2, YFP-SUMO3, and YFP-SUMO5. The bottom panel is a parallel gel stained with Coomassie Brilliant Blue R 250 (CBB) to show the equal loading of protein samples.

**(D)** Upregulation of SUMO3 expression in response to TuMV infection. RNA was isolated from newly emerged leaves at 0, 3, 6, and 9 dpi from Arabidopsis plants inoculated with TuMV-GFP or buffer (as the negative control). ACTIN II was used as the internal control. After normalization with the internal control, the expression levels of SUMO1, SUMO2, SUMO3, SUMO5, and PR1 were calculated relative to the value (which was set to 1) of the negative controls (mock). Error bars denote SD from three experiments (each with three technical replicates).

plant innate immunity (van den Burg et al., 2010). Moreover, a recent study demonstrated that SUMO3 plays an important role in regulating the function of NPR1, a master regulator of plant immunity (Saleh et al., 2015; Liu et al., 2017). Therefore, we analyzed the response of SUMO3 and its paralogs to TuMV infection. Four-week-old wild-type Arabidopsis seedlings were rub-inoculated with a TuMV recombinant clone tagged with GFP (TuMV-GFP) (Huang et al., 2010) using inoculum from TuMV-GFP-infected *N. benthamiana* leaves or buffer only as the negative control. After inoculation, SUMO3 expression was monitored by qRT-PCR at 0, 3, 6, and 9 d postinoculation (dpi) on the inoculated leaf. *PATHOGENESIS-RELATED GENE1* (*PR1*), which is induced in response to infection by a variety of pathogens, served as a molecular marker for the host immunity response. As expected,

the expression of PR1 was markedly upregulated upon TuMV infection at 9 dpi (Figure 1D). The four SUMO paralogs responded differently. SUMO1 and SUMO2 were not affected significantly compared with the nontreated plants (Figure 1D). In contrast, SUMO3 was upregulated and SUMO5 was slightly downregulated (Figure 1D). The expression level of SUMO3 was upregulated ~6-fold at 9 dpi compared with mock-treated plants. These results indicate that the expression of SUMO3 is induced by TuMV infection.

### NIb Interacts with SUMO3

Given that NIb interacts with SCE1 (Xiong and Wang, 2013), we investigated whether NIb also interacts with the four SUMO paralogs. The four SUMO paralogs of Arabidopsis and the TuMV NIb protein (Supplemental Figure 2A) were fused to either the GAL4 DNA binding domain or the GAL4 activation domain and subjected to yeast two-hybrid (Y2H) assays. Arabidopsis SCE1 was used as a positive control (Xiong and Wang, 2013). Yeast strain AH109 harboring SCE1 and NIb positive control plasmids survived on medium lacking tryptophan, leucine, histidine, and adenine, whereas no yeast cells cotransformed with negative control plasmids were recovered, confirming the specificity of the system (Figure 2A). When NIb was coexpressed with each of the four SUMO paralogs, we found that histidine auxotrophy was restored only when NIb was cotransformed with SUMO3, but not with SUMO1, SUMO2, or SUMO5 (Figure 2A), indicating that NIb specifically interacts with SUMO3. To further confirm this result, we performed a bimolecular fluorescence complementation (BiFC) assay (Hu et al., 2002). In this assay, two proteins to be tested for interaction were fused to the two nonfluorescent halves (YN and YC domains) of YFP. The interaction of the two proteins would bring YN and YC together to reconstitute the fluorescence-competent structure, which subsequently gives yellow fluorescence and allows the spatial localization patterns of the protein complexes to be visualized. The four Arabidopsis SUMOs were fused to the C termini of YN and YC, and NIb was fused to the N termini of YN and YC. In cells coexpressing either YN-SUMO3 and NIb-YC or YC-SUMO3 and NIb-YN, YFP fluorescence resulting from the interaction between SUMO3 and NIb was found in both the cytosol and nucleus (Figure 2B). However, no detectable fluorescence was observed in leaf tissue coexpressing NIb-YC with either YN-SUMO1, YN-SUMO2, or YN-SUMO5 under the same conditions (Figure 2B). To investigate whether NIb and SUMO3 undergo direct protein-protein interactions, we performed fluorescence resonance energy transfer (FRET) assays. C-terminal CFP fused to NIb (NIb-CFP) and N-terminal YFP fused to SUMO3 (YFP-SUMO3) were coexpressed in the leaves of *N. benthamiana* and the efficiency of FRET was calculated by confocal microscopy at 2 dpi. YFP-SUMO3 and NIb-CFP interacted with each other, as indicated by a FRET efficiency of 19.18%, which is significantly higher ($P < 0.001$) than that of the negative control (Figure 2C). Taken together, these data suggest that NIb interacts exclusively with SUMO3.

### NIb Is Modified by SUMO3

To determine whether the NIb and SUMO3 interaction could lead to the covalent conjugation of SUMO3 to NIb, we examined the sumoylation status of NIb in planta. C-terminal GFP-tagged NIb (NIb-GFP) and N-terminal FLAG plus 4×Myc tagged SUMO3 (FLAG-4×Myc-SUMO3) were transiently expressed alone or together in *N. benthamiana* leaves by agroinfiltration. At 2 dpi, total proteins were extracted from the infiltrated leaves and incubated with GFP-Trap agarose beads or FLAG M2 monoclonal antibody affinity gel to purify recombinant NIb-GFP or FLAG-4×Myc-SUMO3, respectively. The purified recombinant proteins were then probed with GFP and Myc antibodies. Immunoblotting of proteins purified by GFP-Trap agarose beads with GFP antibodies revealed a protein with the predicted molecular mass of NIb-GFP and additional proteins of higher molecular weights resembling those of NIb-GFP proteins posttranslationally modified in leaf samples expressing NIb-GFP (Figure 2D, left panel). These proteins were not detected in the negative control or in leaves expressing FLAG-4×Myc-SUMO3, suggesting that GFP-Trap agarose beads specifically bind to NIb-GFP. The purified proteins were also probed with Myc antibodies to detect SUMO3-conjugated NIb protein. As shown in Figure 2D (right panel), clear signals with molecular weights higher than the predicted molecular mass of NIb-GFP were detected only in the sample coexpressing NIb-GFP and FLAG-4×Myc-SUMO3. We performed similar immunoblotting experiments to analyze the proteins purified by FLAG M2 monoclonal antibody affinity gel. Immunoblotting using Myc antibodies revealed high levels of SUMO3-modified proteins with various molecular masses in leaf samples expressing FLAG-4×Myc-SUMO3 (Figure 2E, left panel), whereas immunoblotting using GFP antibodies revealed a protein of ~105 kD corresponding to the predicted molecular mass of NIb-GFP (90 kD) modified by FLAG-4×Myc-SUMO3 (15 kD) in the leaf sample coexpressing NIb-GFP and FLAG-4×Myc-SUMO3 (Figure 2E, right panel).

To confirm that NIb is sumoylated by SUMO3 during TuMV infection, we generated the TuMV infectious clone TuMV-GFP/3×HA-NIb, which, upon translation, produces a recombinant NIb tagged with 3×HA at its N terminus (3×HA-NIb). TuMV-GFP/3×HA-NIb had similar infectivity to that of its parental wild-type clone TuMV-GFP, although its induced symptoms were usually delayed for ~2 d in both *N. benthamiana* and Arabidopsis in comparison with those caused by TuMV-GFP. A similar delay in symptoms was also observed for *Tobacco etch virus* when a fluorescent protein, e.g., mCherry, was attached to the N terminus of NIb (Martínez and Daròs, 2014). Tissues of TuMV-GFP/3×HA-NIb infected *N. benthamiana* were used as inoculum to inoculate transgenic Arabidopsis plants expressing an N-terminal FLAG-4×Myc-tagged SUMO3 (SUMO3oe-11; Supplemental Figure 3A). Total proteins from TuMV-GFP/3×HA-NIb-infected or healthy control plants were purified with FLAG M2 monoclonal antibody affinity gel and the purified proteins were detected with polyclonal HA or Myc antibodies. A protein with the predicted size (80 kD) for 3×HA-NIb (65 kD) modified by FLAG-4×Myc-SUMO3 (15 kD) was detected only in virus-infected leaf tissues, but not in healthy control leaf tissues (Figure 2F, middle blot). Taken together, these data indicate that NIb is sumoylated by SUMO3 in planta.

### The Putative SIM2 Is Essential for Sumoylation of NIb

Bioinformatics analysis showed that NIb has three potential sumoylation sites (K148, K172, and K409) and two putative SIMs (Figures 3A and 3B; Supplemental Figure 2A). To locate the

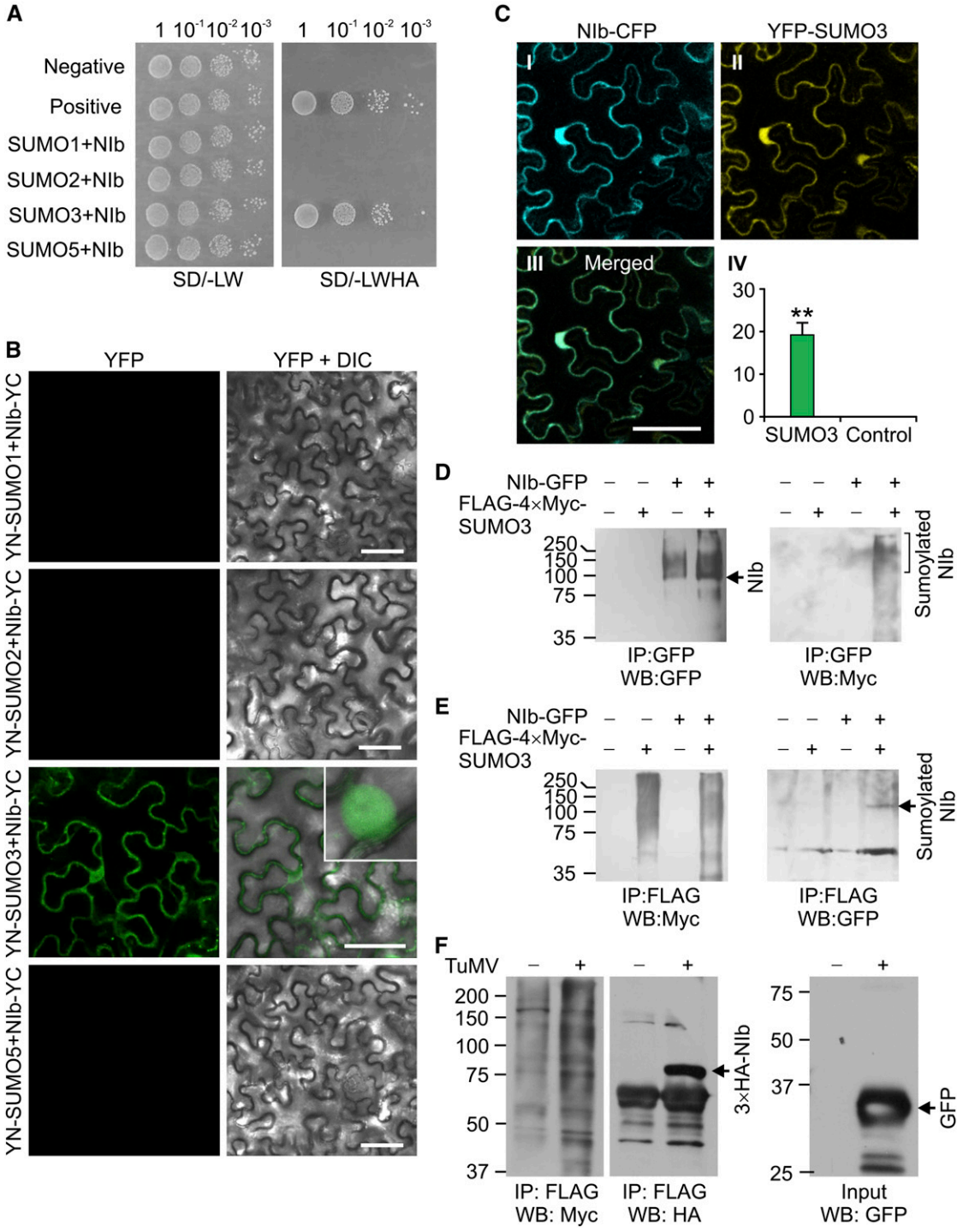


**Figure 2.** NIb Interacts with SUMO3 in Vivo and in Vitro.

**(A)** Y2H assay for protein-protein interactions between NIb and the four Arabidopsis SUMO paralogs. The positive and negative controls are yeast cells cotransformed with pGAD-NIb plus pGBK-SCE1 and pGAD-T plus pGBK-Lam, respectively.

**(B)** BiFC assays of the interactions between NIb and SUMO1, SUMO2, SUMO3, or SUMO5 in *N. benthamiana* leaves. YFP fluorescence (rendered in green) was monitored at 2 dpi. DIC, differential interference contrast. The inset shows typical fluorescent signals from the NIb-SUMO3 interaction in the nucleus. Bars = 50 μm.

domain that interacts with SUMO3, we divided NIb into three fragments: the N-terminal domain (NIb1–143), core domain (NIb144–376), and C-terminal domain (CTD; NIb377–517). The N-terminal domain contains SIM1, core domain contains the two putative sumoylation sites (K148 and K172), and CTD contains the putative sumoylation site (K409) and SIM2 (Supplemental Figure 2B). Y2H and BiFC assays showed that SUMO3 interacts exclusively with the NIb C-terminal domain (Supplemental Figures 2B and 2C), suggesting that SUMO3 might be conjugated to the CTD of NIb.

To further map the sumoylation site(s) in NIb, we constructed NIb mutants in which the lysine residue of each of the three putative SUMO conjugation sites was mutated into arginine individually or together and the conserved residues of the two SIMs were substituted by alanine (Figures 3A and 3B). The resulting mutants were tested for their sumoylation ability using the reconstituted Arabidopsis SUMO pathway in *Escherichia coli* (Okada et al., 2009; Elrouby and Coupland, 2010). After IPTG induction, N-terminal 6×His and thioredoxin (TRX)-tagged NIb (6×His-TRX-NIb) were purified from total protein extracts using Ni-NTA agarose beads. The purified protein sample was further analyzed by immunoblotting with antibodies against TRX. The antibody probes revealed a major band corresponding to the predicted size for 6×His-TRX-NIb, as well as a weaker band of higher molecular weight from IPTG-induced samples, but not in the uninduced sample or the sample with a dysfunctional version of SCE1 [SCE1(C94S)], suggesting this weaker band was SUMO3-modified NIb (Figure 3C). The sumoylated form of NIb was also detected in samples of the K148, K172, or K409 single mutants, the K148/172/409 triple mutant, and the SIM1 mutant NIb(SIM1). The sumoylated form of NIb was absent in NIb(SIM2) (Figure 3C). It is worth mentioning that the level of the sumoylated form of NIb was greatly reduced in the mutants NIb(K409) or NIb(K148/172/409) but not in NIb(K148) and NIb(K172), suggesting that K409 might be a major sumoylation site. The Ni-NTA agarose-purified protein samples were also analyzed by immunoblotting with antibodies against SUMO3. Consistent with the results in Figure 3C, upon IPTG induction, a specific band was present in the NIb samples with functional SCE1, but not in the sample with SCE1(C94S) (Figure 3D). Moreover, upon IPTG induction and in the presence of SCE1, this protein was also evident in the K148, K172, or K409 single mutants, the K148/172/409 triple mutant, and NIb(SIM1) but was absent in NIb(SIM2) (Figure 3D), further supporting the notion that SIM2 is essential for sumoylation of NIb. To further confirm that SIM2 is critical for this process, BiFC and Y2H were performed with wild-type NIb and NIb(SIM2). In contrast to the strong YFP fluorescence in *N. benthamiana* leaf cells coexpressing YN-SUMO3 and NIb-YC, coexpression of YN-SUMO3 and NIb(SIM2)-YC led to very weak fluorescence (Figure 3E). Consistently, NIb almost completely lost its ability to interact with SUMO3 in the Y2H assay when SIM2 was mutated (Figure 3F). Taken together, these data suggest that SIM2 is essential for the NIb-SUMO3 interaction and NIb sumoylation.

### Sumoylation Regulates the Nuclear-Cytoplasmic Partitioning of NIb

To examine the effects of sumoylation on the subcellular localization of NIb, NIb-YFP and NIb(SIM2)-YFP were transiently expressed alone or in the presence of FLAG-4×Myc-SCE1 and FLAG-4×Myc-SUMO3. As a control, NIb was coexpressed with an unrelated protein, FLAG-4×Myc-GUS. NIb-YFP was found in the cytoplasm and predominantly in the nucleus, with uniform distribution in the nucleoplasm and no expression in the nucleolus (Figure 4A, frame I), consistent with previously published data (Restrepo et al., 1990). A similar distribution pattern was observed for the N-terminal YFP-tagged NIb (YFP-NIb) (Supplemental Figure 4). Interestingly, NIb-YFP accumulation in the nucleus was markedly reduced when expressed in the presence of SUMO3 and SCE1 (Figure 4A, frame II). In contrast, the nuclear localization of NIb was not altered when coexpressed with GUS (Figure 4A, frame III). We also analyzed the subcellular localization of NIb(SIM2) under the same conditions. The subcellular localization of NIb(SIM2) was similar to that of NIb when expressed alone (Figure 4A, frame IV). Thus, the mutation of SIM2 has no obvious influence on the nuclear localization of NIb, which is consistent with the previous finding that the nuclear localization of NIb is determined by two nuclear localization signals in the N-terminal and middle domains (Li et al., 1997). Unlike NIb, the mutant NIb(SIM2) showed similar levels of nuclear localization when coexpressed with nonfluorescent protein-tagged SUMO3 and SCE1 or GUS (Figure 4A, frames V and VI). Immunoblotting showed that the reduced levels of NIb in the nucleus, when coexpressed with SCE1 and SUMO3, were not due to the different expression levels (Figure 4B). Together, these results suggest that sumoylation of NIb by SUMO3 affects the accumulation of NIb in the nucleus.

To further confirm that sumoylation affects the nuclear accumulation of NIb, we constructed a permanent sumoylation mimic NIb mutant by fusing the mature form of SUMO3 (1–79

**Figure 2.** (continued).

**(C)** FRET assay for the direct interaction between NIb and SUMO3 in *N. benthamiana* epidermal cells. Panels I to III show fluorescence from SUMO3-CFP, NIb-YFP at 2 dpi, and a merged image of panels I and II, respectively. Panel IV, FRET efficiency between SUMO3 and NIb. Bars represent SD of seven independent FRET analyses in two independent experiments. Asterisks indicate $P < 0.001$ by Student's *t* test. Bar = 50 μm.

**(D)** and **(E)** In vivo immunoprecipitation assays. Total protein was extracted from *N. benthamiana* leaves coinfiltrated with NIb-GFP, FLAG-4×Myc-SUMO3, or NIb-GFP plus FLAG-4×Myc-SUMO3 at 2 dpi and immunoprecipitated with GFP-Trap agarose beads **(D)**, followed by detection with GFP antibodies (left panel) or Myc antibodies (right panel) or immunoprecipitation by FLAG M2 monoclonal antibody affinity gel **(E)** and detection with Myc (left panel) or GFP antibodies (right panel).

**(F)** In vivo coimmunoprecipitation assay. Total proteins were extracted from TuMV-GFP/3×HA-NIb-infected or healthy transgenic Arabidopsis expressing FLAG-4×Myc-SUMO3 and immunoprecipitated by ANTI-FLAG M2 affinity agarose. The purified protein was probed with Myc antibodies (left) and HA antibodies (middle). Total proteins were also detected with GFP antibodies to monitor the infection with TuMV-GFP/3×HA-NIb (right).

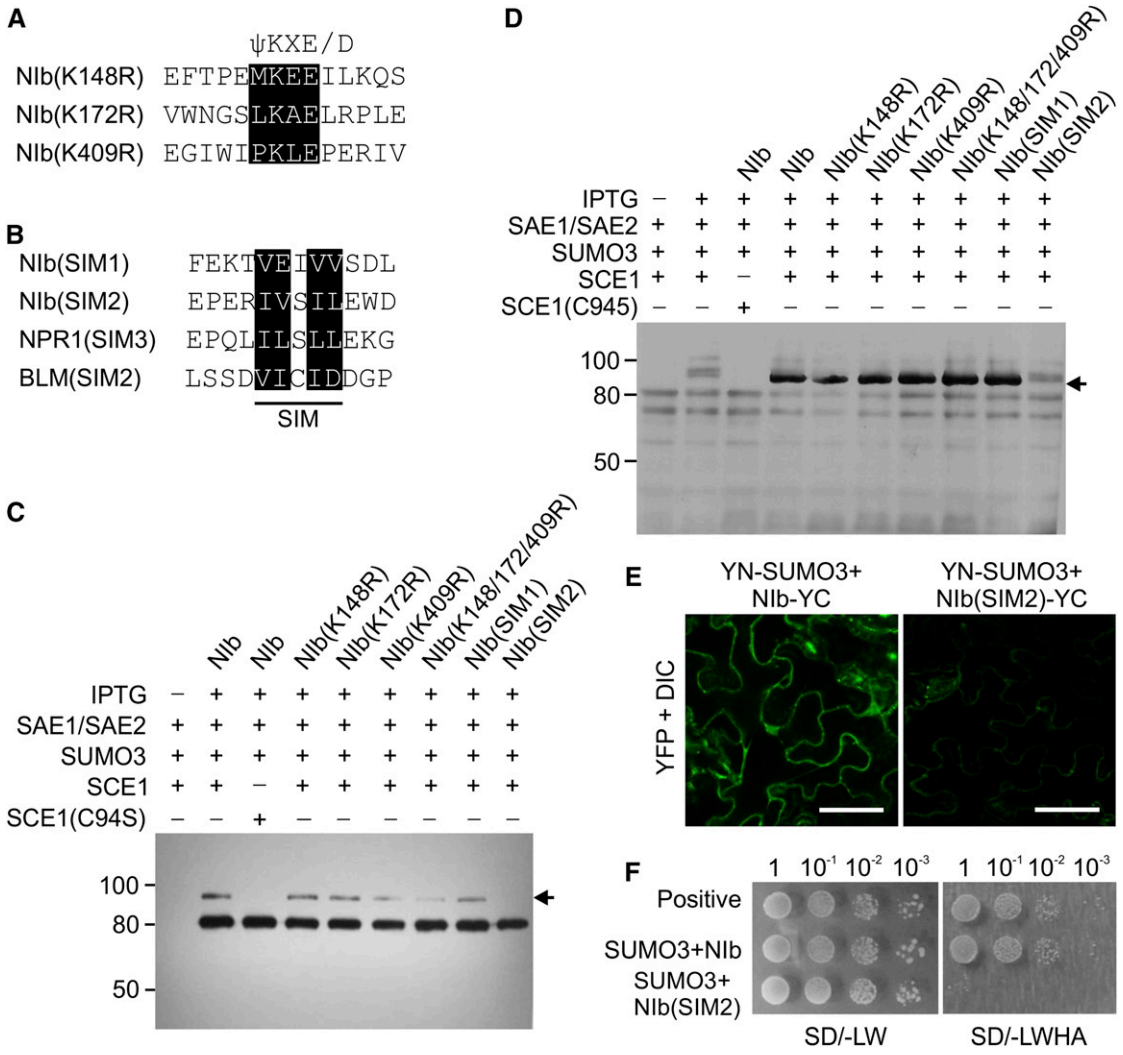


**Figure 3.** The Putative SIM Located in the CTD of NIb Is Required for Sumoylation.

**(A)** Alignment of sumoylation motifs in NIb protein. The predicted sumoylation motifs are highlighted with a black background.
**(B)** Alignment of SUMO-interacting motifs (SIMs) of NIb, NPR1, and BLM (Bloom syndrome, RecQ helicase-like). Conserved amino acids are highlighted with a black background.
**(C)** and **(D)** In vitro sumoylation assay. NIb or NIb mutants were expressed in *E. coli* harboring functional or dysfunctional Arabidopsis sumoylation pathway components, purified with Ni-NTA agarose beads, and detected with antibodies against TRX **(C)** or SUMO3 **(D)**. The sumoylated form of NIb is indicated by an arrowhead.
**(E)** BiFC for protein-protein interactions between SUMO3 and NIb or NIb(SIM2) in *N. benthamiana* epidermal cells at 2 dpi. Bars = 50 μm.
**(F)** Y2H assay for protein-protein interactions between SUMO3 and NIb or NIb(SIM2). The positive control is yeast cotransformed with pGAD-VPg and pGBK-eIF4E (Arabidopsis eukaryotic translation initiation factor 4E).

amino acids, from the first amino acid to the GG cleavage site) to the N terminus of NIb and then deleting the two crucial glycine residues (G92 and G93) of SUMO3 (SUMO3-ΔGG-NIb). This mutant mimics natural sumoylation of lysine residues by covalently linking SUMO to the target protein but disrupts the reversible cleavage to recycle SUMO by the desumoylation enzyme due to the deletion of the two crucial glycine residues (Ross et al., 2002; Bossis et al., 2005; Liu et al., 2016a). Wild-type NIb and SUMO3-ΔGG-NIb (both as a C-terminal YFP-tagged fusion protein) were transiently expressed in *N. benthamiana* leaves. In comparison to the bright fluorescent NIb-YFP signals in the nucleus, the YFP signals of SUMO3-ΔGG-NIb markedly decreased in the nucleus under the same condition (Figure 4C). To confirm the differences in fluorescence between NIb and SUMO3-ΔGG-NIb in the nucleus, we measured the fluorescence intensities of nuclei from 30 cells expressing each of the two proteins. Quantification data showed that the fluorescent intensity of SUMO3-NIb was significantly lower than that of NIb (*t* test, $P < 0.001$; Figure 4D). We purified the nuclei from leaf tissues expressing NIb-YFP or SUMO3-ΔGG-NIb-YFP and conducted

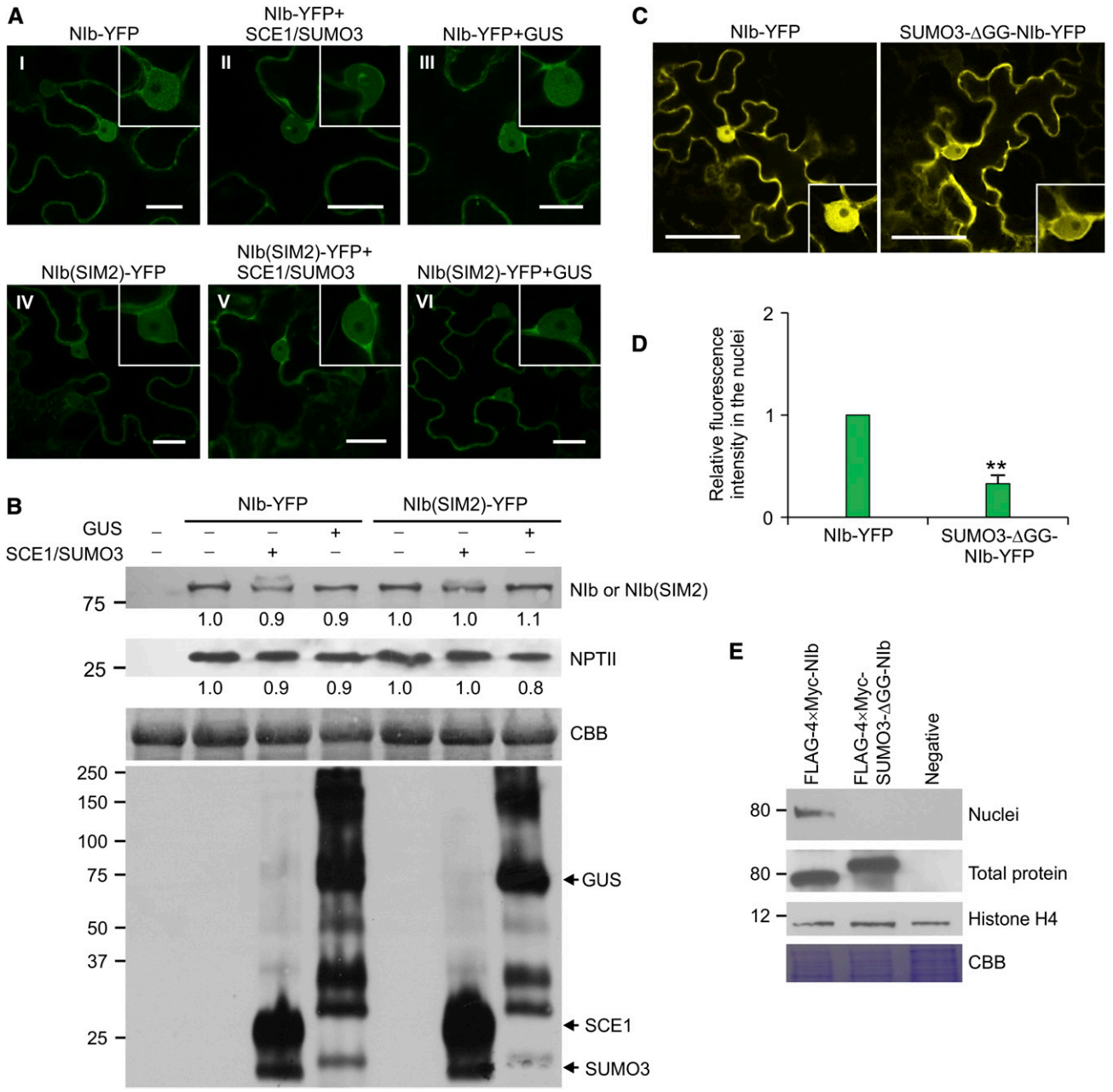


**Figure 4.** Sumoylation Affects the Subcellular Localization of NIb.

**(A)** Comparison of the subcellular localization of NIb-YFP and NIb(SIM2)-YFP (rendered in green) alone or together with nonfluorescent SUMO3 plus SCE1 or with GUS in *N. benthamiana* epidermal cells at 2 dpi. Insets show typical nuclear fluorescent signals from NIb or NIb(SIM2). All frames were taken under a confocal microscope using the same settings. Bars = 20 μm.

**(B)** Immunoblotting analysis of the expression levels of NIb-YFP and NIb(SIM2)-YFP. NIb-YFP and NIb(SIM2)-YFP were detected with GFP antibodies. The expression level of NPTII encoded in both the NIb-YFP and NIb(SIM2)-YFP expression vectors was used as an internal control. A Coomassie blue-stained parallel gel is shown to confirm the equal loading of leaf samples. The expression of SCE1, SUMO3, and GUS was also confirmed by immunoblotting analysis with Myc antibodies.

**(C)** Comparison of the subcellular localization of NIb-YFP (left) and SUMO3-ΔGG-NIb-YFP (right) in *N. benthamiana* epidermal cells. Yellow fluorescence from the recombinant proteins was visualized at 2 dpi under a confocal microscope using the same parameters. Insets show typical nuclear fluorescent signals from NIb-YFP and SUMO3-ΔGG-NIb-YFP. Bars = 50 μm.

**(D)** Quantification of fluorescent signals in the nucleus in *N. benthamiana* epidermal cells expressing NIb-YFP and SUMO3-ΔGG-NIb-YFP using LAS AF Lite (Leica) software. Bars represent SD from two experiments (each with 30 nuclei). Asterisks indicate $P < 0.001$ by Student's *t* test.

**(E)** Immunoblotting analyses of FLAG-4xMyc-NIb and FLAG-4xMyc-SUMO3-ΔGG-NIb in the nuclei and total proteins at 2 dpi probed with FLAG antibodies. Equal loading of the nuclear and total protein samples was monitored by probing with Histone H4 antibodies and CBB staining, respectively.

immunoblotting with antibodies to GFP to detect the two proteins in the nucleus. Since a protein corresponding to the predicted size for free GFP is always detected from plants expressing either NIb-YFP or SUMO3-ΔGG-NIb-YFP, we modified the expression vectors to express N-terminal FLAG-4×Myc tagged NIb (FLAG-4×Myc-NIb) or SUMO3-ΔGG-NIb (FLAG-4×Myc-SUMO3-ΔGG-NIb). At 2 dpi, FLAG-4×Myc-NIb and FLAG-4×Myc-SUMO3-ΔGG-NIb were detected in total protein extracts by immunoblotting with antibodies against FLAG (Figure 4E). The nuclei were purified from the infiltrated leaf tissues. However, FLAG-4×Myc-SUMO3-ΔGG-NIb was not detected in the nuclear extracts using FLAG antibodies, whereas FLAG-4×Myc-NIb was clearly visible. Taken together, these results suggest that sumoylation by SUMO3 might facilitate NIb transport from the nucleus back to the cytoplasm, leading to the reduced NIb levels in the nucleus.

### Knockout or Overexpression of SUMO3 Affects TuMV Infection

To examine the influence of SUMO3 on TuMV infection, a suppressor-mutator transposon insertion mutant of SUMO3 (sumo3-1; SM_3.2707) was obtained from the Nottingham Arabidopsis Stock Centre. This mutant contains a transposon insertion in the third exon, upstream of the G-G motif, which disrupts the expression of SUMO3 from the 78th amino acid (methionine). RT-PCR confirmed that no detectable full-length mRNA is produced by this mutant, suggesting it is a loss-of-function mutant (Figure 5A). In agreement with earlier findings (van den Burg et al., 2010), homozygous sumo3-1 plants exhibited normal growth and development and regular seed germination. Four-week-old wild-type and sumo3-1 plants were then sap-inoculated with TuMV-GFP using leaf extracts from TuMV-GFP-infected *N. benthamiana* as inoculum. The plants were maintained in growth chambers. At 15 dpi, wild-type plants inoculated with TuMV-GFP showed typical TuMV infection symptoms, including yellowing and mottling in leaves and a dwarf, stunted stature, whereas the symptoms in mutant plants were milder (Figure 5B). Furthermore, qRT-PCR showed that TuMV viral RNA levels were reduced by ~80% in the upper leaves of sum3-1 compared with those of wild-type Arabidopsis infected by TuMV-GFP (Figure 5C).

We also generated transgenic Arabidopsis plants expressing N-terminal FLAG-4×Myc-tagged SUMO3 under the control of the *Cauliflower mosaic virus* 35S promoter (Figure 5D). qRT-PCR indicated that SUMO3 was overexpressed (≥2.0-fold) in most independent transgenic lines (15 out of the 20) compared with wild-type plants. However, the transgenic line, SUMO3oe-16, contained lower level of SUMO3 than wild-type plants (Supplemental Figure 3A). Immunoblotting was performed with antibodies against FLAG to confirm the biological activity of FLAG-4×Myc-SUMO3 in three independent transgenic lines. SUMO3-conjugated proteins could only be detected in samples from transgenic plants but not from wild-type Arabidopsis (Supplemental Figure 3B), suggesting that N-terminal FLAG-4×Myc-tagged SUMO3 was expressed and conjugated to cellular proteins in the transgenic plants. Consistent with previous results (van den Burg et al., 2010), none of the SUMO3-overexpressing lines caused a visible developmental phenotype in Arabidopsis, suggesting that SUMO3 is dispensable for normal plant growth under the given conditions. We infected wild-type and six independent transgenic lines showing various expression levels of SUMO3 (namely, SUMO3oe-3, SUMO3oe-7, SUMO3oe-8, SUMO3oe-9, SUMOoe-11, and SUMO3oe-16) with TuMV-GFP and measured viral genomic RNA levels at 15 dpi by qRT-PCR. Transgenic plants with higher expression levels were less susceptible to TuMV and showed milder symptoms than the other lines (Figure 5E). We found a negative correlation between the amount of TuMV-GFP genomic RNA and SUMO3 expression levels (Figure 5F).

To corroborate this observation, we prepared protoplasts using leaves from wild-type, sumo3-1, and SUMO3-overexpressing Arabidopsis (line SUMO3oe-9) plants and conducted a TuMV transfection assay with wild-type TuMV-GFP; the replication-defective clone TuMV-GFP/ΔGDD was used as a control to monitor the basal transcriptional level of the 35S promoter. In this replication-defective clone, the conserved GDD motif of NIb was substituted with alanine, which disrupts RdRp catalytic activity. At 24 h after transfection, the protoplasts were harvested for RNA extraction and the levels of TuMV negative (–) and positive (+) strand RNA were evaluated by qRT-PCR. The replication efficiency was determined based on the fold changes in TuMV-GFP RNA to TuMV-GFP/ΔGDD RNA. The levels of both + and – stranded genomic RNA of TuMV were significantly reduced in protoplasts isolated from sumo3-1 and SUMO3-overexpressing Arabidopsis (Figure 5G). These results suggest that either knockout or overexpression of SUMO3 inhibits TuMV replication in Arabidopsis.

### Sumoylation Is Necessary for TuMV Replication

To investigate the effects of sumoylation on TuMV infection, we constructed the TuMV mutant clone TuMV-GFP/NIb(SIM2), which, upon translation, produces a sumoylation-defective form of NIb. This mutant and its parental clone TuMV-GFP were inoculated into *N. benthamiana* seedlings by agroinfiltration. The plants were maintained in a growth chamber to monitor symptom development for a period of 20 d. *N. benthamiana* infected with TuMV-GFP showed typical TuMV symptoms as early as 5 to 6 d after agroinfiltration. Plants infiltrated with TuMV-GFP/NIb(SIM2) remained symptomless throughout the observation period (Figure 6A). No TuMV-GFP/NIb(SIM2) genomic RNA could be detected in the newly emerging leaves by qRT-PCR (Figure 6B).

We also constructed a TuMV infectious clone (TuMV-SUMO3-ΔGG-NIb) in which NIb is permanently sumoylated, and another infectious clone encoding a CFP at the N terminus of NIb (TuMV-CFP-NIb) as a control (Figure 6C). These clones, as well as TuMV-GFP or mCherry-tagged TuMV (TuMV-6K2mCherry; Cotton et al., 2009), were inoculated into *N. benthamiana* seedlings by agroinfiltration or by sap inoculation after propagation in *N. benthamiana*. Plants infected with TuMV-GFP and TuMV-6K2mCherry showed typical TuMV symptoms, such as curling and yellowing of upper leaves and stunted stature, at 5 to 6 d after agroinfiltration or 4 to 5 d after sap inoculation. The symptoms in *N. benthamiana* plants caused by TuMV-CFP-NIb were slightly milder than those caused by TuMV-GFP (Figure 6D), and the

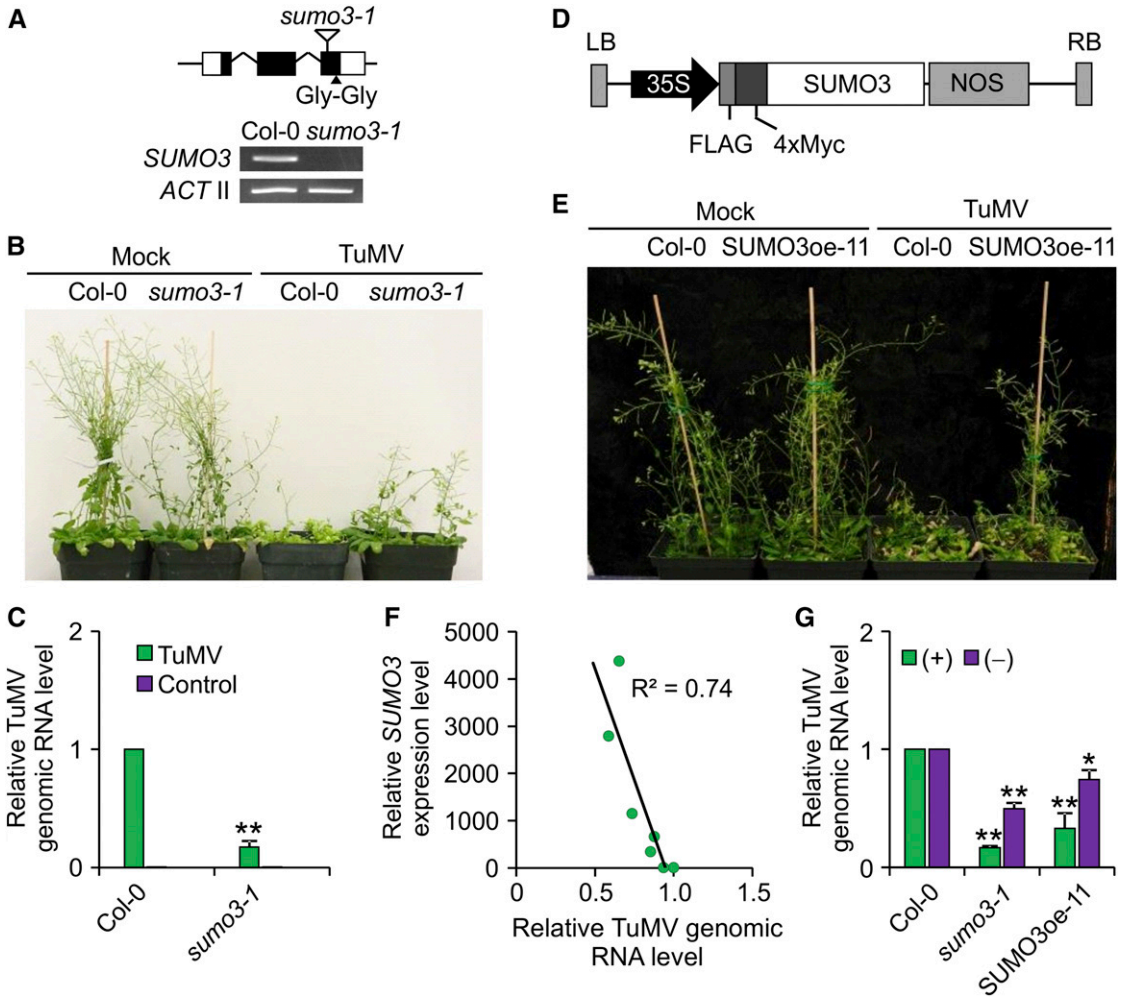


**Figure 5.** SUMO3 Affects TuMV Replication.

**(A)** Schematic diagram of sumo3-1 (upper panel) and RT-PCR analysis of the expression of SUMO3 in sumo3-1 (lower panel). Exons, introns, and 5′ and 3′ untranslated regions are represented by boxes, bent lines, and white boxes, respectively. The suppressor-mutator transposon is indicated by an arrowhead, and the Gly-Gly motif is indicated by a solid arrowhead.

**(B)** Phenotypes of wild-type and sumo3-1 after TuMV infection at 15 dpi.

**(C)** qRT-PCR analysis of TuMV genomic RNA accumulation in the upper leaves of wild-type and sumo3-1 at 15 dpi. ACTIN II was used as the internal control. The level of TuMV genomic RNA in wild-type was normalized to 1. Bar represents SD of three experiments (each with five technical replicates).

**(D)** Diagram of the T-DNA region in the plasmid used to generate transgenic Arabidopsis plants. LB, 35S, FLAG, 4×Myc, SUMO3, NOS, and RB represent the left border of T-DNA, 35S promoter, FLAG tag, 4×Myc tag, SUMO3 protein coding region, NOS terminator, and right border of T-DNA, respectively.

**(E)** Phenotypes of wild-type and SUMO3-overexpressing transgenic Arabidopsis (SUMO3oe-11) infected by TuMV at 15 dpi.

**(F)** The relationship between the level of TuMV genomic RNA and that of SUMO3 mRNA in seven SUMO3oe lines. The relative levels of SUMO3 mRNA (*y* axis) and TuMV genomic RNA (*x* axis) in the SUMOoe lines were obtained by normalization against their respective level in wild-type Arabidopsis. The correlation was statistically significant ($R^2 = 0.74$; $P < 0.01$).

**(G)** Accumulation of TuMV-GFP positive (+) and negative (–) strand of genomic RNA in protoplasts isolated from wild-type Col-0, sumo3-1, and SUMO3-overexpressing transgenic Arabidopsis. ACTIN II was used as the internal control, and TuMV-GFP/ΔGDD was used to show the basal transcriptional level of the 35S promoter. The relative level of TuMV genomic RNA in wild-type Col-0 was set to 1. Error bars represent SD from three experiments (each with five technical replicates). **$P < 0.001$ and *$P < 0.05$ to the amount of the corresponding TuMV genomic RNA in Col-0 by Student's *t* test, respectively.

symptoms induced by TuMV-CFP-NIb were delayed by ~6 d (with agroinfiltration) and 2 d (with sap inoculation) compared with those caused by TuMV-GFP and TuMV-6K2mCherry, respectively (Figure 6D). Plants infected by TuMV-SUMO3-ΔGG-NIb showed a further delay in symptoms (Figure 6D). The development of distinguishable symptoms caused by TuMV-SUMO3-ΔGG-NIb was delayed by ~15 d (agroinfiltration) and 5 d (sap inoculation) compared with that of the wild-type controls TuMV-GFP or TuMV-6K2mCherry (Figure 6D). Moreover, TuMV-SUMO3-ΔGG-NIb only caused slight yellowing of upper new leaves. The relative viral

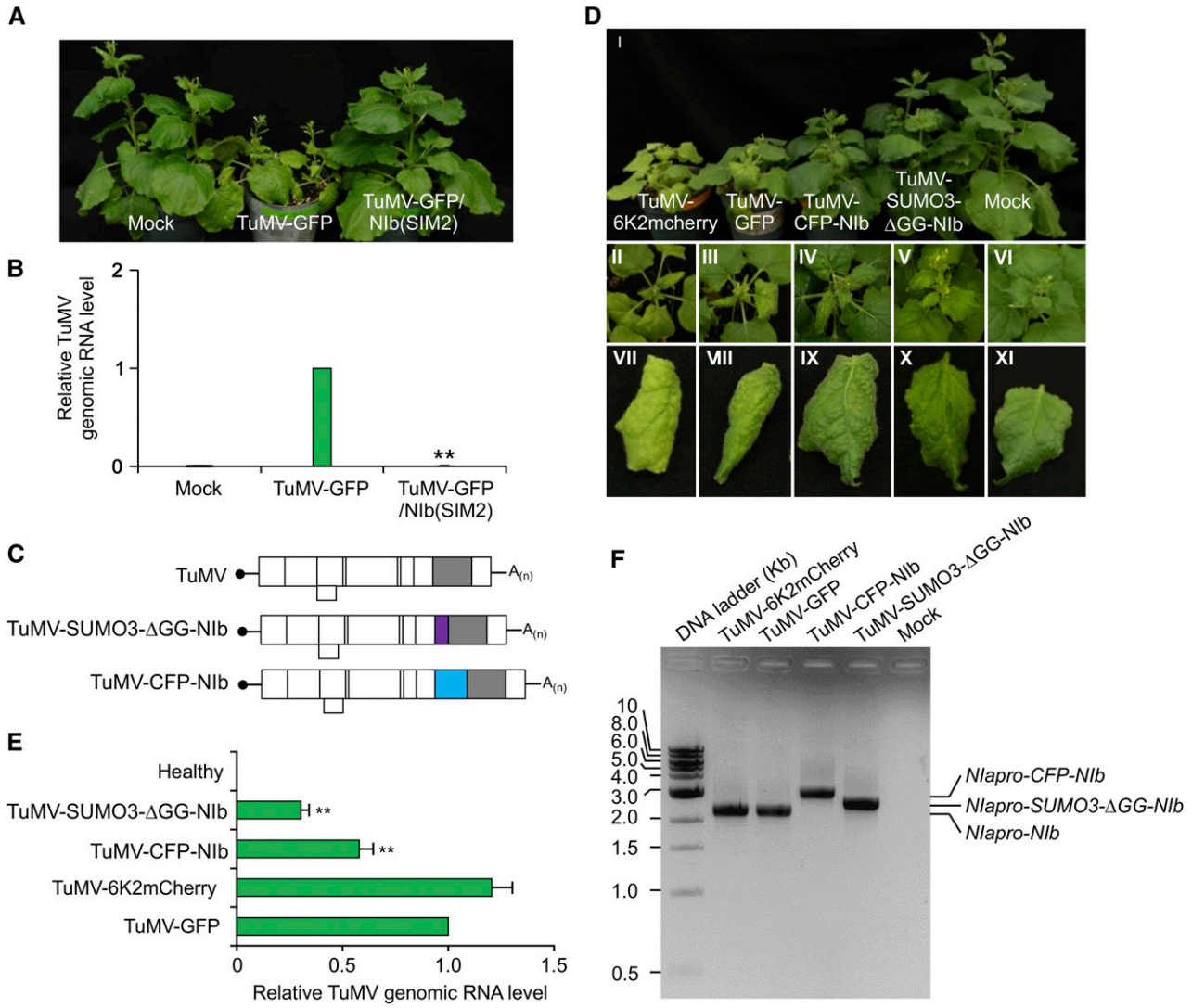


**Figure 6.** Sumoylation by SUMO3 Is Crucial for TuMV Infectivity.

**(A)** Phenotypes of *N. benthamiana* plants infected by TuMV-GFP and TuMV-GFP/NIb(SIM2) at 20 dpi.

**(B)** qRT-PCR analysis of TuMV-GFP and TuMV-GFP/NIb(SIM2) genomic RNA accumulation in *N. benthamiana* at 20 dpi. The *N. benthamiana* ACTIN gene (AY179605) was used as the internal control. TuMV-GFP genomic RNA in *N. benthamiana* was normalized to 1. Asterisks indicate $P < 0.001$ to the amount of TuMV-GFP genomic RNA by Student's *t* test.

**(C)** Schematic representation of TuMV, TuMV-CFP-NIb, and TuMV-SUMO3-ΔGG-NIb. NIb, SUMO3, and CFP are indicated as gray, purple, and cyan rectangles, respectively.

**(D)** Phenotypes of *N. benthamiana* plants inoculated with TuMV-6K2mCherry, TuMV-GFP, TuMV-CFP-NIb, and TuMV-SUMO3-ΔGG-NIb at 20 dpi.

**(E)** qRT-PCR analysis TuMV-6K2mCherry, TuMV-GFP, TuMV-CFP-NIb, and TuMV-SUMO3-ΔGG-NIb genomic RNA accumulation in *N. benthamiana* at 20 dpi. The *N. benthamiana* ACTIN gene was used as the internal control. TuMV-GFP genomic RNA level in *N. benthamiana* was normalized to 1. Bars represent SD of three experiments.

**(F)** RT-PCR detection of genomic fragments covering the NIa-NIb region in the recombinant viruses on systematically infected leaves at 20 dpi. CFP and SUMO3 were inserted at the NIa-NIb junction in the recombinant viruses TuMV-CFP-NIb and TuMV-SUMO3-ΔGG-NIb, respectively. The sizes of DNA markers and amplified cDNA fragments are indicated.

genomic RNA levels in these plants were monitored by qRT-PCR. Viral genomic RNA accumulation was severely reduced in plants infected by TuMV-SUMO3-ΔGG-NIb versus TuMV-CFP or TuMV-GFP (Figure 6E). Subsequent sequencing of viruses from upper new leaves confirmed that both TuMV-CFP-NIb and TuMV-SUMO3-ΔGG-NIb were stably inherited by progeny viruses in *N. benthamiana* plants (Figure 6F). Taken together, these data suggest that sumoylation of NIb is necessary for the successful infection of *N. benthamiana* and that permanent sumoylation of NIb inhibits viral infection.

### Sumoylation of NIb by SUMO3 Suppresses the Host Immunity Response

As SUMO3 expression is upregulated in response to TuMV infection (Figure 1D) and to immunity stimulators such as flg22 peptide and salicylic acid (van den Burg et al., 2010; this study) and since SUMO3 is involved in regulating the function of NPR1 (Saleh et al., 2015), we reasoned that the NIb-SUMO3 interaction might interfere with the host immune response. To address this hypothesis, we compared the basic immunity levels of wild-type, sumo3-1, and three SUMO3 transgenic lines (SUMO3oe-8, SUMO3oe-11, and SUMO3oe-16) by analyzing the expression of PR1 and PR2. SUMO3oe-8 and SUMO3oe-11 are two overexpression lines, and SUMO3oe-16 is a knockdown line (Supplemental Figure 3A). qRT-PCR revealed low levels of expression of both PR1 and PR2 in wild-type Arabidopsis. Interestingly, the expression of PR1 and PR2 was barely detectable in sumo3-1 plants (Figure 7A), suggesting that SUMO3 is required for maintaining the basal levels of expression of PR genes. In contrast, PR1 and PR2 were upregulated in the two SUMO3 overexpression transgenic lines, but not in the SUMO3 knockdown line.

Next, we examined the immunity responses of the wild type, sumo3-1, and SUMO3oe-11 to TuMV-GFP infection. In wild-type and sumo3-1 plants, TuMV-GFP upregulated PR1 expression by ~11- and 30-fold at 20 dpi, respectively (Figure 7B). Interestingly, the expression level of PR1 in TuMV-GFP-infected SUMO3oe-11 plants was reduced to 30% that of mock (buffer)-treated SUMO3oe-11 seedlings (Figure 7B). Therefore, the TuMV infection-induced expression of PR1 is negatively regulated by SUMO3 expression.

To further investigate NIb protein, we generated transgenic Arabidopsis plants expressing N-terminal FLAG-4×Myc tagged NIb (FLAG-4×Myc-NIb). We determined the expression levels of NIb in 13 randomly selected independent transgenic lines by qRT-PCR (Supplemental Figure 5A). The expression of NIb was confirmed by immunoblotting in three lines with higher expression levels (NIb-6, NIb-8, and NIb-9; Supplemental Figure 5B). All 13 transgenic lines had normal phenotypes like that of wild-type Arabidopsis plants, suggesting that the expression of the NIb transgene has no obvious effect on Arabidopsis development. qRT-PCR showed that the expression of PR1 was reduced in all three NIb transgenic lines compared with wild-type plants (Figure 7C). To determine if the suppression of PR1 expression by NIb is sumoylation dependent, we produced transgenic Arabidopsis plants expressing FLAG-4×Myc-NIb(SIM2) (Supplemental Figures 5C and 5D). The transgenic plants exhibited similar phenotypes to that of wild-type Arabidopsis. PR1 expression levels were higher in the NIb(SIM2) transgenic lines than in wild-type plants. Taken together, these data suggest that the sumoylation of NIb by SUMO3 suppresses the host immune response.

## DISCUSSION

In a recent study, we found that the NIb protein of TuMV interacts with SCE1, the only SUMO-conjugating enzyme of Arabidopsis, and that the NIb-SCE1 interaction is crucial for TuMV infection (Xiong and Wang, 2013). These findings prompted us to investigate whether NIb is sumoylated by one or more of the four

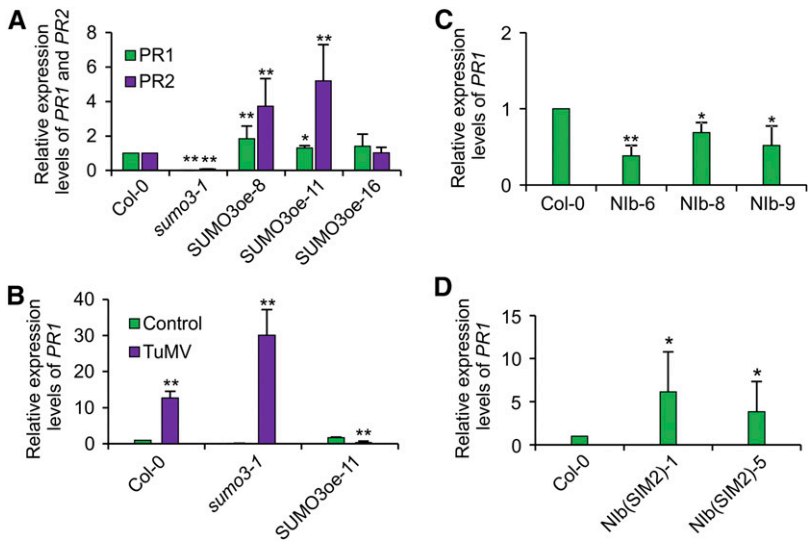


**Figure 7.** Sumoylation by SUMO3 Is Required by NIb to Suppress the Host Immune Response.

**(A)** The expression levels of PR1 and PR2 in 2-week-old Col-0, sumo3-1, and SUMO3oe transgenic plants. ACTIN II was used as the internal control. The expression levels of PR1 and PR2 in Col-0 were normalized to 1. Error bars represent SD of five biological repeats. **P < 0.001 and *P < 0.01.

**(B)** qRT-PCR analysis of PR1 expression in Col-0, sumo3-1, and SUMO3oe-11 plants infected with TuMV-GFP at 20 dpi. ACTIN II was used as the internal control. The expression of PR1 in control Col-0 plants was normalized to 1. Error bars represent SD of five biological repeats. **P < 0.001 by Student's *t* test.

**(C)** qRT-PCR analysis of PR1 expression in Col-0 wild-type and NIb transgenic plants. Error bars represent SD of five experiments with a total of 30 2-week-old seedlings. The expression of PR1 in control Col-0 plants was normalized to 1. **P < 0.001 and *P < 0.01.

**(D)** qRT-PCR analysis of PR1 expression in Col-0 and NIb(SIM2) transgenic plants by qRT-PCR. Error bars represent SD of five experiments with a total of 50 2-week-old seedlings. The expression of PR1 in control Col-0 plants was normalized to 1. *P < 0.01 by Student's *t* test.

SUMO paralogs and how the sumoylation of NIb affects viral infection. In this study, we found that despite the fact that SUMO1 and SUMO2 are the most abundantly expressed and most efficiently conjugated SUMOs among all known SUMOs in Arabidopsis (Saracco et al., 2007; van den Burg et al., 2010; Castaño-Miquel et al., 2011), NIb exclusively interacted with SUMO3 (Figure 2). Moreover, the expression of SUMO3 was upregulated by TuMV infection (Figure 1D). These data are in agreement with our recent finding that sumoylation plays an essential role in potyviral infection (Xiong and Wang, 2013).

Given that both the NIb-interacting proteins SCE1 and SUMO3 are required for sumoylation and TuMV infection, we investigated whether NIb is sumoylated. Due to the transient and reversible nature of sumoylation, detecting the sumoylated form of a particular protein is very difficult (Sánchez-Durán et al., 2011; Xiong and Wang, 2013). We recently demonstrated that NIb could undergo sumoylation in an *E. coli* strain harboring the reconstituted SUMO conjugation pathway (Elrouby and Coupland, 2010; Xiong and Wang, 2013). In this study, we successfully detected the sumoylated forms of NIb derived from plant leaves transiently overexpressing SUMO3 and NIb simultaneously and under TuMV infection (Figure 2). These data strongly suggest that NIb is sumoylated in plants. Sumoylation occurs on the lysine residue within the conserved motif (ψ-K-X-E/D) in the target protein via a SUMO E3 ligase (Melchior, 2000; Bernier-Villamor et al., 2002), and SUMOs can interact with SIMs of target proteins noncovalently (Kerscher, 2007). Bioinformatics analysis predicted that there are three conserved sumoylation sites and two SIMs within the NIb protein (Figure 3; Supplemental Figure 2). Indeed, substitution of the conserved residues in SIM2 with alanine compromised NIb sumoylation (Figures 3C and 3D), suggesting that SIM2 is required for this process. Moreover, multiple sequence alignment showed that SIM2 is highly conserved among potyviruses (Supplemental Figure 6), supporting the notion that sumoylation plays a conserved role in the potyvirus life circle. In addition, we found that sumoylation of NIb mutants NIb(K409R) and NIb(K148/172/409R) but not NIb(K148R) and NIb(K172R) was markedly inhibited in the in vitro sumoylation assay (Figure 3C). These data suggest that K409 is a primary sumoylation site. This suggestion is supported by the observation that K409 is in close proximity to SIM2 and is conserved in all potyviruses analyzed in this study (Supplemental Figure 6A). To determine whether K409 is essential for TuMV infection, we generated a TuMV K409R mutant clone. Indeed, our infection assay revealed that the K409R substitution indeed compromised TuMV infectivity (Supplemental Figure 6B.)

Unlike SUMO1 and SUMO2, which can form poly-SUMO chains on target proteins, SUMO3 can only be attached to target proteins as a monomer or as the terminal unit of the poly-SUMO chain, as SUMO3 itself lacks an internal sumoylation motif (Colby et al., 2006). Therefore, the multiple forms of sumoylated NIb observed in this work (Figure 2D) more likely represent NIb that has been monosumoylated by SUMO3 at different Lys residues in the conserved or nonconserved sumoylation sites. This may explain the observation that sumoylation was not completely abolished when all three putative sumoylation sites were mutated (Figure 3D). However, we cannot exclude the possibility that the sumoylated NIb was also modified simultaneously by other posttranslational modification mechanisms, such as phosphorylation, ubiquitination, and acylation.

Sumoylation can affect the function of the target protein in many ways, such as its stability, subcellular localization, and interacting partner. For instance, sumoylation has been suggested to stabilize NS5, the RdRp of DENV (Su et al., 2016), and the 3D polymerase of EV71 (Liu et al., 2016b). Sumoylation is thought to occur mainly in the nucleus, since SCE1, the only SUMO-conjugating enzyme of Arabidopsis, localizes to the nucleus (Xiong and Wang, 2013), and most sumoylated proteins discovered thus far are nuclear proteins (Geiss-Friedlander and Melchior, 2007; Elrouby and Coupland, 2010). Wild-type NIb, the only RdRp encoded by TuMV, is a well-known nuclear protein (Restrepo et al., 1990). However, when coexpressed with SCE1 and SUMO3 (to enhance sumoylation), the nuclear accumulation of wild-type NIb, but not its sumoylation-defective mutant NIb(SIM2), was dramatically reduced (Figure 4A). Moreover, the permanent sumoylation mimic NIb mutant SUMO3-ΔGG-NIb mainly accumulated in the cytoplasm, with little detected in the nucleus (Figures 4C to 4E). Thus, sumoylation of NIb by SUMO3 may regulate the nuclear-cytoplasmic partitioning of NIb. As potyviruses assemble the viral replication complex in association with cellular membranes exclusively in the cytoplasm (Wei and Wang, 2008; Wei et al., 2010a, 2013), such cytoplasm-preferential partitioning may be required for viral infection. Recently, the nuclear targeting protein P20 of *Bamboo mosaic virus* was found to interact with the major nuclear protein fibrillarin in the nucleus to form the ribonucleoprotein complex, which mediates long-distance trafficking of *Bamboo mosaic virus*-associated satellite RNAs (Chang et al., 2016). It would be interesting to

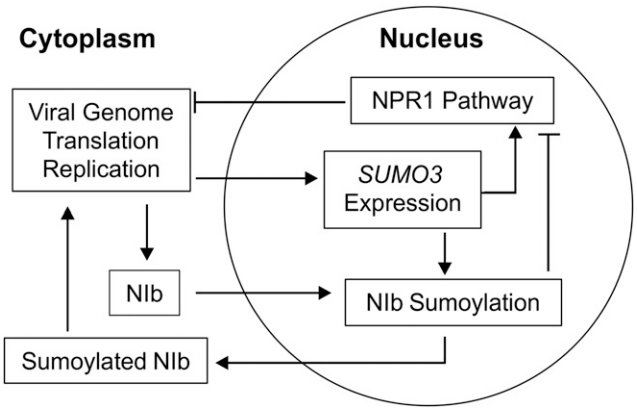


**Figure 8.** Proposed Model for the Possible Role of NIb Sumoylation by SUMO3 in Potyviral Infection.

After translation of the potyviral genome, the potyviral NIb targets (and accumulates in) the nucleus (Restrepo et al., 1990; Esteban et al., 2003). In the nucleus, NIb interacts with SCE1 and SUMO3 and is sumoylated by SUMO3 (Xiong and Wang, 2013; this study). Simultaneously, potyviral infection upregulates SUMO3 expression (this study), and SUMO3 activates the NPR1 resistance pathway (Saleh et al., 2015). The sumoylation of NIb by SUMO3 may compete for or deplete SUMO3 in the nucleus, and as a result, activation of the NPR1-mediated immune response is suppressed (this study). The sumoylated form of NIb in the nucleus retargets the cytoplasm to promote viral replication (this study).

determine how these protein or ribonucleoprotein complexes move out of the nucleus.

In this study, we analyzed TuMV replication in wild-type, SUMO3 knockout, and SUMO3-overexpressing plants and compared the infectivity of TuMV infectious clones containing either a sumoylation-defective or a permanently sumoylated form of NIb. Our results showed that knockout of SUMO3 attenuated TuMV replication, and mutation of SIM2 in NIb completely abolished TuMV replication, suggesting that SUMO3 is an important host factor for TuMV replication. However, overexpression of SUMO3 also inhibited TuMV replication (Figures 5E and 5F), and TuMV infectivity was greatly attenuated when wild-type NIb was replaced with a permanently sumoylated form of NIb (Figures 6D and 6E). This was unexpected since overexpression of a host factor of viral pathogens usually promotes viral infection (Wang, 2015; Nagy, 2016). SUMO3 is involved in regulating plant immunity (Lois et al., 2003; Saleh et al., 2015). Knockout of SUMO3 eliminated the basal expression of PR genes, and overexpression of SUMO3 upregulated PR expression (Figure 7A; van den Burg et al., 2010). Excessive SUMO3 protein in transgenic plants might preactivate host antiviral immunity to TuMV. This is also consistent with our observation that viral replication was negatively correlated with the expression level of SUMO3 (Figure 5F). Thus, our results suggest that SUMO3 plays dual roles as a host factor of TuMV and as an antiviral defender.

Another interesting finding of this study is that overexpression of NIb but not its sumoylation-defective mutant NIb(SIM2) in transgenic plants suppressed PR1 expression (Figures 7C and 7D), suggesting that NIb functions as a viral suppressor of the host defense response to counteract the SUMO3-activated NPR1-mediated defense pathway in TuMV-infected plants. In agreement with this suggestion, TuMV infection induced a significantly lower level of PR1 gene expression in SUMO3-overexpressing plants than in wild-type plants (Figure 7B), implying that TuMV can suppress the expression of the host antiviral response through SUMO3. However, TuMV infection induced a much higher level of PR1 expression in sumo3-1 seedlings than in wild-type plants (Figure 7A), suggesting that alternative pathways exist that activate PR gene expression. If this is the case, how does NIb utilize SUMO3 to suppress host antiviral responses? In virus-infected plants, potyviral NIb accumulates in the nucleus (Restrepo et al., 1990; Esteban et al., 2003), where it is sumoylated. Sumoylation of NIb by SUMO3 might compete for or deplete SUMO3 in the nucleus, which is required to activate the NPR1 resistance pathway (Saleh et al., 2015). As a result, activation of the NPR1-mediated immune response to the upregulation of SUMO3 by viral infection is suppressed.

Based on the above discussion, we propose a model describing the possible function of the sumoylation of NIb by SUMO3 (Figure 8). After translation in the cytoplasm, NIb targets and accumulates in the nucleus where NIb is sumoylated by SUMO3. After sumoylation, NIb is exported from the nucleus into the cytoplasm, possibly together with host factor(s), to promote viral infection. Along with potyviral infection, SUMO3 expression is upregulated, which could suppress viral infection via the SUMO3-activated NPR1-mediated defense pathway. This host defense response is counteracted by high-level accumulation of NIb in the nucleus. Therefore, SUMO3 dynamically regulates potyviral infection via sumoylation of NIb and the plant defense response via sumoylation of NPR1.

## METHODS

### Plant Materials and Virus Inoculations

The *Arabidopsis thaliana* and *Nicotiana benthamiana* plants were grown in pots in a growth chamber under a 16-/8-h photoperiod with an average light intensity of 120 $\mu$mol $m^{-2}$ $s^{-1}$ provided by cool-white fluorescence tubes (Philips Fluorescent T8) at 23°C and 60% humidity. The suppressor-mutator transposon insertion line (sumo3-1; accession code SM_3.2707) was obtained from the Nottingham Arabidopsis Stock Centre. The SUMO3, NIb, and NIb(SIM2) overexpression lines were transformed into Arabidopsis ecotype Col-0 by the floral dip method (Bent, 2006). Progeny seeds were screened by direct spraying with 20 mg/L Basta solutions. For agroinfiltration, agrobacteria carrying viral infectious clones were infiltrated into *N. benthamiana* leaves at an $OD_{600}$ of 0.5. For sap inoculation, virally infected *N. benthamiana* leaves were ground in 10 mM phosphate buffer, pH 7.2, and the extract was used to directly rub-inoculate *N. benthamiana* or Arabidopsis plants predusted with carborundum. After 2 to 3 min, the inoculated leaves were rinsed with distilled water. Inoculated plants were returned to the growth chamber and assessed for symptom development.

### Phylogenetic Analysis

The protein sequences of Arabidopsis and human SUMOs and Arabidopsis POLYUBIQUITIN14 (UBQ14) were downloaded from the GenBank database in the National Center for Biotechnology Information. Multiple alignment of amino acid sequences was performed using ClustalW program (Thompson et al., 1994) with Gonnet protein weight matrix and multiple alignment gap penalty of 10 and gap extension penalty 0.1. The phylogenetic tree was constructed using MEGA7 software (Kumar et al., 2016) with the neighboring-joining method (Saitou and Nei, 1987). Phylogeny was tested using the bootstrap method (1000 replications), P-distance amino acid substitution model, and uniform rates of evolution.

### Plasmid Construction

Unless otherwise noted, all plasmids used in this work were constructed using Gateway technology (Invitrogen). All plasmids were verified by DNA sequencing. The full coding sequences of SUMO1, SUMO2, SUMO3, SUMO5, and SCE1 in Arabidopsis and NIb in TuMV were amplified with Phusion DNA polymerase (NEB). The amplified DNA fragments were transferred by recombination into the entry vector pDONR221 or pENTR (Invitrogen) using Gateway BP Clonase II Enzyme mix (Invitrogen) following the supplier's instructions. The NIb arginine substitution mutants NIb(K148R), NIb(K172R), NIb(K409R), and NIb(K148/172/409R) and the alanine substitution mutants NIb(SIM1) and NIb(SIM2) in which four conserved residues were substituted by alanine were generated using a Quickchange mutagenesis II kit (Agilent Technologies Canada) using pDONR-NIb as the template. To construct the deconjugation-deficient NIb mutant (SUMO3-ΔGG-NIb), the sequence encoding the mature form of SUMO3 (1–279 nucleotides) was amplified with Phusion DNA polymerase and inserted into the pGEM-T Easy vector (Promega) to generate plasmid pGEM-SUMO3. The NIb coding sequence was then recombined in frame downstream of SUMO3 in pGEM-SUMO3. After substitution of the Gly-Gly motif in SUMO3 with double alanine using a QuickChange II XL site-directed mutagenesis kit (Stratagene), the chimeric gene was amplified with Gateway-compatible primers and recombined into pDONR221, resulting in the plasmid pDONR-SUMO3-ΔGG-NIb. For yeast-two-hybrid analysis, SUMO1, SUMO2, SUMO3, SUMO5, SCE1, or NIb and its mutants in the pDONR221 vector were inserted into the Gateway-compatible yeast two-hybrid vectors

pGBKT7-DEST and pGADT7-DEST (Lu et al., 2010) by recombination with Gateway LR Clonase Enzyme mix (Invitrogen). For transient expression in *N. benthamiana*, the target gene in pDONR221 was recombined into the Gateway-compatible pEarleyGate-101 (or pGWB441), -102, or -103 plant expression vector (Earley et al., 2006) to produce C-terminal YFP, CFP, or GFP-tagged fusion constructs, or inserted into the Gateway-compatible pEarleyGate-201, -104, pGWB515 (Nakagawa et al., 2007), pET32-gateway (Elrouby and Coupland, 2010), or pBA-FLAG-4myc-DC vector (Zhu et al., 2011) to yield the N-terminal HA, YFP, 3×HA, Thx-6×Histidine, or FLAG-4×Myc-tagged constructs. For the BiFC assay, genes of interest were recombined into Gateway-compatible BiFC p35S-gatewayYN, p35S-gatewayYC, p35S-YNgateway, or p35S-YCgateway vectors (Lu et al., 2010). All plasmids were confirmed by DNA sequencing.

To construct a TuMV infectious clone that contains a permanently sumoylated form of NIb (TuMV-SUMO3-ΔGG-NIb), the fragment encoding SUMO3-ΔGG-NIb was amplified using pDONR-SUMO3-ΔGG-NIb as a template and fused to the C terminus of NIa by overlapping PCR. This fragment was then ligated into the pCRTM4Blunt-TOPO vector (Invitrogen) to construct pBlunt-NIa-SUMO3-ΔGG-NIb. After confirmation by DNA sequencing, this fragment was digested by *Mfe*I and *Nde*I and inserted into the corresponding sites of plasmid pBlunt-TuMV5k to construct pBlunt-TuMV5k:NIa-SUMO3-ΔGG-NIb. pBlunt-TuMV5k was created by inserting the 5-kb *Sna*BI-*Mlu*I fragment of TuMV into pCR-Blunt vector. The pBlunt-TuMV5k:NIa-SUMO3-ΔGG-NIb was then digested with *Sna*BI and *Mlu*I, and the resulting 5 kb fragment was then inserted back into the same sites of the infectious clone TuMV-GFP (Wei et al., 2013) to construct the clone TuMV-SUMO3-ΔGG-NIb.

To construct the TuMV infectious clone TuMV-CFP-NIb containing N-terminal CFP-fused NIb, the sequence encoding CFP was amplified using pEarleyGate-102 as a template and inserted into the position between NIa and NIb using the cloning strategy described above.

To construct a TuMV infectious clone containing N-terminal 3×HA-fused NIb (TuMV-GFP/3×HA-NIb), the sequence encoding 3×HA-NIb was amplified from pGWB515-NIb and inserted into the junction of NIa and NIb using the cloning strategy described above.

To construct a TuMV infectious clone containing sumoylation-defective NIb [TuMV-GFP/NIb(SIM2)] or a K409 to R mutation [TuMV-GFP/NIb(K409R)], the SIM2 or K409 of NIb in pBlunt-TuMV5k was mutated with a QuikChange II XL site-directed mutagenesis kit (Agilent technologies). After confirmation by DNA sequencing, the resulting plasmids pBlunt-TuMV5k/NIb(SIM2) and pBlunt-TuMV5k/NIb(K409R) were digested with *Sna*BI and *Mlu*I, and the fragment containing the mutated NIb was inserted back into the same sites of the infectious clone TuMV-GFP to construct TuMV-GFP/NIb(SIM2) and TuMV-GFP/NIb(K409R). All primers used in this study are listed in Supplemental Table 1.

### Yeast Two-Hybrid and Quantitative β-Galactosidase Assays

The yeast two-hybrid constructs were introduced into yeast strain AH109 (Clontech) using the lithium acetate method as described previously (Xiong and Wang, 2013; Zhang et al., 2015). Cells were plated onto selective medium lacking Trp and Leu, and putative transformants were transferred to medium lacking Trp, Leu, His, and adenine. The quantitative β-galactosidase assay was performed as described (Mockli and Auerbach, 2004).

### Nucleus Purification

Nuclei were purified as described previously with some modifications (Gendrel et al., 2005). In brief, ~2 g of *N. benthamiana* leaves were harvested at 2 d after agroinfiltration and ground to a fine powder in liquid nitrogen. The powder was combined with 30 mL of extraction buffer 1 (0.4 M sucrose, 10 mM Tris-HCl, pH 8.0, 10 mM $MgCl_2$, 5 mM β-mercaptoethanol, 0.1 mM PMSF, and two tablets of Complete Protease Inhibitor [Roche]). After filtration through two layers of Miracloth, the solution was centrifuged at 3000*g* for 20 min. After resuspension in 1 mL of extraction buffer 2 (0.25 M sucrose, 10 mM Tris-HCl, pH 8.0, 10 mM $MgCl_2$, 5 mM β-mercaptoethanol, 0.1 mM PMSF, 1% Trion X-100, and one tablet of complete mini protease inhibitor), the solution was centrifuged at 12,000*g* for 10 min. The pellet was resuspended thoroughly in 400 μL of extraction buffer 3 (1.7 M sucrose, 10 mM Tris-HCl, pH 8.0, 2 mM $MgCl_2$, 5 mM β-mercaptoethanol, 0.1 mM PMSF, 0.15% Triton X-100, and one tablet of complete mini protease inhibitor). The resuspended pellet was transferred to a fresh microcentrifuge tube containing 400 μL of 2.5 M sucrose, carefully layered with 400 μL of extraction buffer 3, and centrifuged at 16,000*g* for 1 h. The pellet containing nuclei was resuspended in 100 μL of nucleus storage buffer (50 mM Tris-HCl, pH 8.0, 0.3 mM sucrose, 5 mM $MgCl_2$, and 5 mM β-mercaptoethanol) and stored at −80°C or immediately subjected to SDS-PAGE. All operations were performed at 4°C or on ice.

### Protein Work

For total protein extraction, *N. benthamiana* or Arabidopsis tissues were ground into a fine powder in liquid nitrogen and resuspended in a fivefold volume of protein extraction buffer (50 mM Tris-HCl, pH 7.5, 0.15 M NaCl, 1 mM EDTA, 0.1% Tween 20, and 10% glycerol) (Leister et al., 2005). The crude lysate was centrifuged at 12,000*g* for 10 min at 4°C, and the supernatant was stored in 80°C until use or directly used for SDS-PAGE. The protein concentration was determined using the Bradford assay (Bio-Rad) with a standard curve calculated from serially diluted BSA solutions.

For immunoblotting analysis, 15 μg of total protein per lane was separated on a 10% polyacrylamide gel or an 8 to 16% Mini-PROTEAN TGXTM precast polyacrylamide gel (Bio-Rad). After electrophoresis, the proteins were transferred to polyvinylidene fluoride membrane using a Trans-Blot SD Semi-Dry Transfer Cell (Bio-Rad). After blocking for 2 h in PBST (50 mM Tris-HCl, pH 7.5, 150 mM NaCl, and 0.05% Tween 20) with 5% nonfat dry milk at room temperature, the membranes were incubated with the appropriate antibodies overnight at 4°C or 2 h at room temperature. These primary antibodies included rabbit anti-HA (catalog number H6908; Sigma-Aldrich Canada) at 1: 2000 dilution, rabbit anti-Myc (catalog number ab9106; Abcam Canada) at 1:5000 dilution, rabbit anti-GFP N-terminal antibody (catalog number G1544; Sigma-Aldrich) at 1:5000 dilution, mouse anti-FLAG tag (catalog number F3165; Sigma-Aldrich) at 1:5000 dilution, rabbit anti-SUMO3 (catalog number ab5317; Abcam) at 1:2000 dilution, rabbit anti-Neomycin Phosphotransferase II (NPTII) at 1:1000 (catalog number 06-747; Millipore Canada), and rabbit ant-histone H4 (catalog number 07-108; Millipore) at 1:10,000. The membranes were washed six times with PBST and incubated with the proper secondary antibodies (Sigma-Aldrich) for 2 h at room temperature. After washing six times with PBST, the membranes were visualized with Immobilon Western chemiluminescent HRP substrate (Millipore) following the manufacturer's instructions. In each experiment, a parallel gel was stained with Coomassie Brilliant Blue R 250 as the loading control.

For immunoprecipitation, *N. benthamiana* leaves (~5 g) were harvested and ground to a powder in liquid nitrogen. Ground tissues were resuspended in 15 mL of IP buffer (50 mM Tris, pH 8.0, 150 mM NaCl, 1% Triton X-100, 0.05% SDS, 0.5 mM EDTA, and two tablets of Complete Protease Inhibitor [Roche]). The crude lysate was centrifuged at 20,000*g* for 15 min at 4°C. After centrifugation, 1 mL of supernatant was filtered through 70 μm Fisherbrand Nylon mesh (Fisher Scientific) and incubated with 20 μL of FLAG M2 monoclonal antibody affinity gel (Sigma-Aldrich), monoclonal Anti-HA-Agarose (Sigma-Aldrich), or GFP-Trap agarose beads (ChromoTek; distributed by Bulldog Bio). After 2 h incubation at 4°C, the agarose beads were collected by centrifugation, washed at least three times with IP buffer, and resuspended in 50 μL 1× SDS-PAGE loading buffer. After boiling for 5 min at 95°C, 10 μL of supernatant was separated by 10% polyacrylamide gel electrophoresis and transferred to nitrocellulose membranes. Immunoprecipitated proteins were detected by immunoblot analysis with the proper antibodies as described above. Relative quantification of proteins was performed by densitometric analysis using GelAnalyzer 2010 software

(http://www.gelanalyzer.com/) according to the instructions provided. All immunoblotting analyses were repeated at least three times.

### Fluorescence Analysis

Binary plasmids were transformed into *Agrobacterium tumefaciens* strain GV3101, and transient expression in *N. benthamiana* leaves was achieved through agroinfiltration. The fluorescence of YFP and CFP was visualized with a Leica TCS SP5 2 confocal laser scanning microscope as described previously (Wei et al., 2010b; Cheng et al., 2015). The FRET experiment was performed as described previously (Xiong and Wang, 2013). To record multiple fluorescent signals, the sequential mode was used to minimize signal bleed-through, and each fluorescent signal was further confirmed separately. Fluorescence intensity in the confocal images was quantified using LAS AF Lite software (Leica).

### In Vitro Sumoylation Assays

The in vitro *Escherichia coli* sumoylation assay was performed as described previously (Elrouby and Coupland, 2010; Xiong and Wang, 2013). The human in vitro sumoylation assay was performed using a SUMOylation assay kit (Abcam) according to the instructions provided.

### RT-PCR

Total RNA was isolated from Arabidopsis or *N. benthamiana* leaf tissues using an RNeasy Plant Mini Kit (Qiagen) as instructed. Four hundred micrograms of RNA was used as the template for first-strand cDNA synthesis with oligo(dT) 12-18 primer using Superscript III reverse transcriptase (Invitrogen). RT-PCR amplification was performed in a 20 $\mu$L volume containing 4 $\mu$L of 50-fold diluted cDNA, 5 $\mu$M each primer, and 1$\times$ SYBR Green PCR Mix (Bio-Rad). Relative transcript abundance was estimated using Bio-Rad CFX Manager software. The genomic RNA of TuMV was determined by amplification of a 257-bp fragment of the TuMV CP gene, and the Arabidopsis ACTIN II gene or *N. benthamiana* ACTIN gene (NbACTIN) was used as an internal control. Primers are listed in Supplemental Table 1. For all qRT-PCR except otherwise stated, leaf samples of four individual plants from the same treatment were pooled as a technical replicate. Each experiment consisted of five biological replicates and was repeated at least three times.

### Arabidopsis Protoplast Preparation and Transfection

Arabidopsis protoplasts were prepared using well-expanded leaves from 4-week-old seedlings of wild-type Col-0, sumo3-1, or SUMO3 overexpression transgenic line (SUMO3oe-9) as described (Deng et al., 2015; Yoo et al., 2007). Protoplasts were transfected with TuMV-GFP and GDD mutant (TuMV-GFP/$\Delta$GDD) via DNA-PEG-calcium transfection (Cheng et al., 2015; Deng et al., 2015). Twenty-four hours after transfection, the protoplasts were harvested for RNA extraction.

### Accession Numbers

Sequence data from this article can be found in the GenBank/EMBL libraries under the following accession numbers: AT4G26840 (SUMO1), AT5G55160 (SUMO2), AT5G55170 (SUMO3), AT2G32765 (SUMO5), AT3G18780 (Arabidopsis ACTIN II), AT3G57870 (SCE1), AT4G02890 (UBQ14), AT1G64280 (NPR1), AT2G14610 (PR1), AT3G57260 (PR2), NM_003352 (HsSUMO1), NM_006937 (HsSUMO2), NM_006936 (HsSUMO3), NM_001002255 (HsSUMO4), AY179605 (NbACTIN), and NC_002509 (TuMV strain UK1).

### Supplemental Data

**Supplemental Figure 1.** Phylogenetic relationship between Arabidopsis and human SUMOs.

**Supplemental Figure 2.** SUM03 interacts with NIb at the C-terminal domain.

**Supplemental Figure 3.** Analysis of SUM03 expression in transgenic Arabidopsis.

**Supplemental Figure 4.** Subcellular localization of NIb-YFP and YFP-NIb in *N. benthamiana* epidermal cells at 2 dpi.

**Supplemental Figure 5.** Expression of NIb and NIb(SIM2) in transgenic Arabidopsis.

**Supplemental Figure 6.** Characterization of K409.

**Supplemental File 1.** Alignment used to produce the phylogenetic tree shown in Supplemental Figure 1.

**Supplemental Table 1.** List of primers used in this study.

## ACKNOWLEDGMENTS

We thank Peter Nagy for valuable comments and advice on this work. We thank Nabil Elrouby and George Coupland for the pET32b Gateway vector and the *E. coli* sumoylation assay system, Yuhai Cui for the modified Gateway vectors of pGADT7, pGBKT7, p35S-YN, and p35SYC, Alex Molnar for photography and artwork, and Jamie McNeil for technical support. This work was supported in part by an A-base grant from Agriculture and Agri-Food Canada and a discovery grant from the Natural Sciences and Engineering Research Council of Canada to A.W.

## AUTHOR CONTRIBUTIONS

X.C., R.X., and A.W. designed the project. X.C., R.X., Y.L., and F.L. conducted the experiments. All authors analyzed the data. X.C., R.X., and A.W. wrote the article.

Received October 11, 2016; revised January 27, 2017; accepted February 17, 2017; published February 21, 2017.

## REFERENCES

**Bent, A.** (2006). *Arabidopsis thaliana* floral dip transformation method. In Agrobacterium Protocols, K. Wang, ed (Totowa, NJ: Humana Press), pp. 87–104.

**Bernier-Villamor, V., Sampson, D.A., Matunis, M.J., and Lima, C.D.** (2002). Structural basis for E2-mediated SUMO conjugation revealed by a complex between ubiquitin-conjugating enzyme Ubc9 and RanGAP1. Cell **108:** 345–356.

**Bossis, G., Malnou, C.E., Farras, R., Andermarcher, E., Hipskind, R., Rodriguez, M., Schmidt, D., Muller, S., Jariel-Encontre, I., and Piechaczyk, M.** (2005). Down-regulation of c-Fos/c-Jun AP-1 dimer activity by sumoylation. Mol. Cell. Biol. **25:** 6964–6979.

**Budhiraja, R., Hermkes, R., Müller, S., Schmidt, J., Colby, T., Panigrahi, K., Coupland, G., and Bachmair, A.** (2009). Substrates related to chromatin and to RNA-dependent processes are modified by Arabidopsis SUMO isoforms that differ in a conserved residue with influence on desumoylation. Plant Physiol. **149:** 1529–1540.

**Camborde, L., Planchais, S., Tournier, V., Jakubiec, A., Drugeon, G., Lacassagne, E., Pflieger, S., Chenon, M., and Jupin, I.** (2010). The ubiquitin-proteasome system regulates the accumulation of Turnip yellow mosaic virus RNA-dependent RNA polymerase during viral infection. Plant Cell **22:** 3142–3152.

**Castaño-Miquel, L., Seguí, J., and Lois, L.M.** (2011). Distinctive properties of Arabidopsis SUMO paralogues support the in vivo predominant role of AtSUMO1/2 isoforms. Biochem. J. **436:** 581–590.

**Castillo, A.G., Kong, L.J., Hanley-Bowdoin, L., and Bejarano, E.R.** (2004). Interaction between a geminivirus replication protein and the plant sumoylation system. J. Virol. **78:** 2758–2769.

**Chang, C.H., Hsu, F.C., Lee, S.C., Lo, Y.S., Wang, J.D., Shaw, J., Taliansky, M., Chang, B.Y., Hsu, Y.H., and Lin, N.S.** (2016). The nucleolar fibrillarin protein is required for helper virus-independent long-distance trafficking of a subviral satellite RNA in plants. Plant Cell **28:** 2586–2602.

**Cheng, X.F., Deng, P., Cui, H., and Wang, A.** (2015). Visualizing double-stranded RNA distribution and dynamics in living cells by dsRNA binding-dependent fluorescence complementation. Virology **485:** 439–451.

**Chenon, M., Camborde, L., Cheminant, S., and Jupin, I.** (2012). A viral deubiquitylating enzyme targets viral RNA-dependent RNA polymerase and affects viral infectivity. EMBO J. **31:** 741–753.

**Chung, B.Y., Miller, W.A., Atkins, J.F., and Firth, A.E.** (2008). An overlapping essential gene in the Potyviridae. Proc. Natl. Acad. Sci. USA **105:** 5897–5902.

**Colby, T., Matthäi, A., Boeckelmann, A., and Stuible, H.P.** (2006). SUMO-conjugating and SUMO-deconjugating enzymes from Arabidopsis. Plant Physiol. **142:** 318–332.

**Cotton, S., Grangeon, R., Thivierge, K., Mathieu, I., Ide, C., Wei, T., Wang, A., and Laliberté, J.F.** (2009). Turnip mosaic virus RNA replication complex vesicles are mobile, align with microfilaments, and are each derived from a single viral genome. J. Virol. **83:** 10460–10471.

**Deng, P., Wu, Z., and Wang, A.** (2015). The multifunctional protein CI of potyviruses plays interlinked and distinct roles in viral genome replication and intercellular movement. Virol. J. **12:** 141.

**Dye, B.T., and Schulman, B.A.** (2007). Structural mechanisms underlying posttranslational modification by ubiquitin-like proteins. Annu. Rev. Biophys. Biomol. Struct. **36:** 131–150.

**Earley, K.W., Haag, J.R., Pontes, O., Opper, K., Juehne, T., Song, K., and Pikaard, C.S.** (2006). Gateway-compatible vectors for plant functional genomics and proteomics. Plant J. **45:** 616–629.

**Elrouby, N., and Coupland, G.** (2010). Proteome-wide screens for small ubiquitin-like modifier (SUMO) substrates identify Arabidopsis proteins implicated in diverse biological processes. Proc. Natl. Acad. Sci. USA **107:** 17415–17420.

**Esteban, O., García, J.A., Gorris, M.T., Domínguez, E., and Cambra, M.** (2003). Generation and characterisation of functional recombinant antibody fragments against RNA replicase NIb from Plum pox virus. Biochem. Biophys. Res. Commun. **301:** 167–175.

**Everett, R.D., Boutell, C., and Hale, B.G.** (2013). Interplay between viruses and host sumoylation pathways. Nat. Rev. Microbiol. **11:** 400–411.

**Gao, S., et al.** (2015). Interaction of NS2 with AIMP2 facilitates the switch from ubiquitination to sumoylation of M1 in Influenza A virus-infected cells. J. Virol. **89:** 300–311.

**Geiss-Friedlander, R., and Melchior, F.** (2007). Concepts in sumoylation: a decade on. Nat. Rev. Mol. Cell Biol. **8:** 947–956.

**Gendrel, A.V., Lippman, Z., Martienssen, R., and Colot, V.** (2005). Profiling histone modification patterns in plants using genomic tiling microarrays. Nat. Methods **2:** 213–218.

**Gurer, C., Berthoux, L., and Luban, J.** (2005). Covalent modification of Human immunodeficiency virus type 1 p6 by SUMO-1. J. Virol. **79:** 910–917.

**Hu, C.D., Chinenov, Y., and Kerppola, T.K.B.** (2002). Visualization of the interactions among bZIP and Rel family protein in living cells using bimolecular fluorescence complementation. Mol. Cell **9:** 789–798.

**Huang, T.S., Wei, T., Laliberté, J., and Wang, A.** (2010). A host RNA helicase-like protein, AtRH8, interacts with the potyviral genome-linked protein, VPg, associates with the virus accumulation complex, and is essential for infection. Plant Physiol. **152:** 255–266.

**Jakubiec, A., Drugeon, G., Camborde, L., and Jupin, I.** (2007). Proteolytic processing of Turnip yellow mosaic virus replication proteins and functional impact on infectivity. J. Virol. **81:** 11402–11412.

**Kerscher, O.** (2007). SUMO junction-what's your function? EMBO Rep. **8:** 550–555.

**Kerscher, O., Felberbaum, R., and Hochstrasser, M.** (2006). Modification of proteins by ubiquitin and ubiquitin-like proteins. Annu. Rev. Cell Dev. Biol. **22:** 159–180.

**Kim, S.H., Palukaitis, P., and Park, Y.I.** (2002). Phosphorylation of Cucumber mosaic virus RNA polymerase 2a protein inhibits formation of replicase complex. EMBO J. **21:** 2292–2300.

**Koonin, E.V.** (1991). The phylogeny of RNA-dependent RNA polymerases of positive-strand RNA viruses. J. Gen. Virol. **72:** 2197–2206.

**Kumar, S., Stecher, G., and Tamura, K.** (2016). MEGA7: Molecular evolutionary genetics analysis version 7.0 for bigger datasets. Mol. Biol. Evol. **33:** 1870–1874.

**Kurepa, J., Walker, J.M., Smalle, J., Gosink, M.M., Davis, S.J., Durham, T.L., Sung, D.Y., and Vierstra, R.D.** (2003). The small ubiquitin-like modifier (SUMO) protein modification system in Arabidopsis: accumulation of SUMO1 and -2 conjugates is increased by stress. J. Biochem. **278:** 6862–6872.

**Leister, R.T., Dahlbeck, D., Day, B., Li, Y., Chesnokova, O., and Staskawicz, B.J.** (2005). Molecular genetic evidence for the role of SGT1 in the intramolecular complementation of Bs2 protein activity in *Nicotiana benthamiana*. Plant Cell **17:** 1268–1278.

**Li, X.H., Valdez, P., Olvera, R.E., and Carrington, J.C.** (1997). Functions of the Tobacco etch virus RNA polymerase (NIb): subcellular transport and protein-protein interaction with VPg/proteinase (NIa). J. Virol. **71:** 1598–1607.

**Liu, Q., Ning, Y., Zhang, Y., Yu, N., Zhao, C., Zhan, X., Wu, W., Chen, D., Wei, X., Wang, G.-L., Cheng, S., and Cao, L.** (2017). OsCUL3a negatively regulates cell death and immunity by degrading OsNPR1 in rice. Plant Cell **29:** 345–359.

**Liu, Y., Lai, J., Yu, M., Wang, F., Zhang, J., Jiang, J., Hu, H., Wu, Q., Lu, G., Xu, P., and Yang, C.** (2016a). The Arabidopsis SUMO E3 ligase AtMMS21 dissociates the E2Fa/DPa complex in cell cycle regulation. Plant Cell **28:** 2225–2237.

**Liu, Y., Zheng, Z., Shu, B., Meng, J., Zhang, Y., Zheng, C., Ke, X., Gong, P., Hu, Q., and Wang, H.** (2016b). SUMO modification stabilizes enterovirus 71 polymerase 3D to facilitate viral replication. J. Virol. **90:** 10472–10485.

**Lois, L.M., Lima, C.D., and Chua, N.-H.** (2003). Small ubiquitin-like modifier modulates abscisic acid signaling in Arabidopsis. Plant Cell **15:** 1347–1359.

**Lu, Q., Tang, X., Tian, G., Wang, F., Liu, K., Nguyen, V., Kohalmi, S.E., Keller, W.A., Tsang, E.W.T., Harada, J.J., Rothstein, S.J., and Cui, Y.** (2010). Arabidopsis homolog of the yeast TREX-2 mRNA export complex: components and anchoring nucleoporin. Plant J. **61:** 259–270.

**Martínez, F., and Daròs, J.A.** (2014). Tobacco etch virus protein P1 traffics to the nucleolus and associates with the host 60S ribosomal subunits during infection. J. Virol. **88:** 10725–10737.

**Melchior, F.** (2000). SUMO-nonclassical ubiquitin. Annu. Rev. Cell Dev. Biol. **16:** 591–626.

**Mockli, N., and Auerbach, D.** (2004). Quantitative beta-galactosidase assay suitable for high-throughput applications in the yeast two-hybrid system. Biotechniques **36:** 872–876.

**Nagy, P.D.** (2016). Tombusvirus-host interactions: co-opted evolutionarily conserved host factors take center court. Annu. Rev. Virol. **3:** 491–515.

**Nakagawa, T., et al.** (2007). Improved gateway binary vectors: high-performance vectors for creation of fusion constructs in transgenic analysis of plants. Biosci. Biotechnol. Biochem. **71:** 2095–2100.

**Novatchkova, M., Budhiraja, R., Coupland, G., Eisenhaber, F., and Bachmair, A.** (2004). SUMO conjugation in plants. Planta **220:** 1–8.

**Okada, S., Nagabuchi, M., Takamura, Y., Nakagawa, T., Shinmyozu, K., Nakayama, J.I., and Tanaka, K.** (2009). Reconstitution of *Arabidopsis thaliana* SUMO pathways in *E. coli*: functional evaluation of SUMO machinery proteins and mapping of sumoylation sites by mass spectrometry. Plant Cell Physiol. **50:** 1049–1061.

**Olspert, A., Chung, B.Y., Atkins, J.F., Carr, J.P., and Firth, A.E.** (2015). Transcriptional slippage in the positive-sense RNA virus family Potyviridae. EMBO Rep. **16:** 995–1004.

**Restrepo, M.A., Freed, D.D., and Carrington, J.C.** (1990). Nuclear transport of plant potyviral proteins. Plant Cell **2:** 987–998.

**Revers, F., and García, J.A.** (2015). Molecular biology of potyviruses. In Advances in Virus Research, Vol. 92, M. Karl and C.M. Thomas, eds (San Diego, CA: Academic Press), pp. 101–199.

**Rodamilans, B., Valli, A., Mingot, A., San León, D., Baulcombe, D., López-Moya, J.J., and García, J.A.** (2015). RNA polymerase slippage as a mechanism for the production of frameshift gene products in plant viruses of the Potyviridae family. J. Virol. **89:** 6965–6967.

**Ross, S., Best, J.L., Zon, L.I., and Gill, G.** (2002). SUMO-1 modification represses Sp3 transcriptional activation and modulates its subnuclear localization. Mol. Cell **10:** 831–842.

**Saitou, N., and Nei, M.** (1987). The neighboring-joining method: A new method for reconstructing phylogenetic trees. Mol. Biol. Evol. **4:** 406–425.

**Saleh, A., Withers, J., Mohan, R., Marqués, J., Gu, Y., Yan, S., Zavaliev, R., Nomoto, M., Tada, Y., and Dong, X.** (2015). Post-translational modifications of the master transcriptional regulator NPR1 enable dynamic but tight control of plant immune responses. Cell Host Microbe **18:** 169–182.

**Sánchez-Durán, M.A., Dallas, M.B., Ascencio-Ibañez, J.T., Reyes, M.I., Arroyo-Mateos, M., Ruiz-Albert, J., Hanley-Bowdoin, L., and Bejarano, E.R.** (2011). Interaction between geminivirus replication protein and the SUMO-conjugating enzyme is required for viral infection. J. Virol. **85:** 9789–9800.

**Saracco, S.A., Miller, M.J., Kurepa, J., and Vierstra, R.D.** (2007). Genetic analysis of sumoylation in Arabidopsis: conjugation of SUMO1 and SUMO2 to nuclear proteins is essential. Plant Physiol. **145:** 119–134.

**Sloan, E., Tatham, M.H., Groslambert, M., Glass, M., Orr, A., Hay, R.T., and Everett, R.D.** (2015). Analysis of the SUMO2 proteome during HSV-1 infection. PLoS Pathog. **11:** e1005059.

**Su, C.I., Tseng, C.H., Yu, C.Y., and Lai, M.M.C.** (2016). SUMO modification stabilizes Dengue virus nonstructural protein 5. J. Virol. **90:** 4308–4319.

**Thompson, J.D., Higgins, D.G., and Gibson, T.J.** (1994). CLUSTAL W: improving the sensitivity of progressive multiple sequence alignment through sequence weighting, position-specific gap penalties and weight matrix choice. Nucleic Acids Res. **22:** 4673–4680.

**Urcuqui-Inchima, S., Haenni, A.L., and Bernardi, F.** (2001). Potyvirus proteins: a wealth of functions. Virus Res. **74:** 157–175.

**van den Burg, H.A., Kini, R.K., Schuurink, R.C., and Takken, F.L.W.** (2010). Arabidopsis small ubiquitin-like modifier paralogs have distinct functions in development and defense. Plant Cell **22:** 1998–2016.

**Varadaraj, A., Mattoscio, D., and Chiocca, S.** (2014). SUMO Ubc9 enzyme as a viral target. IUBMB Life **66:** 27–33.

**Wang, A.** (2015). Dissecting the molecular network of virus-plant interactions: The complex roles of host factors. Annu. Rev. Phytopathol. **53:** 45–66.

**Wei, T., Huang, T.S., McNeil, J., Laliberté, J., Hong, J., Nelson, R.S., and Wang, A.** (2010a). Sequential recruitment of the endoplaasmic reticulum and chloroplasts for plant potyvirus replication. J. Virol. **84:** 799–809.

**Wei, T., and Wang, A.** (2008). Biogenesis of cytoplasmic membranous vesicles for plant potyvirus replication occurs at endoplasmic reticulum exit sites in a COPI- and COPII-dependent manner. J. Virol. **82:** 12252–12264.

**Wei, T., Zhang, C., Hong, J., Xiong, R., Kasschau, K.D., Zhou, X., Carrington, J.C., and Wang, A.** (2010b). Formation of complexes at plasmodesmata for potyvirus intercellular movement is mediated by the viral protein P3N-PIPO. PLoS Pathog. **6:** e1000962.

**Wei, T., Zhang, C., Hou, X., Sanfaçon, H., and Wang, A.** (2013). The SNARE protein Syp71 is essential for Turnip mosaic virus infection by mediating fusion of virus-induced vesicles with chloroplasts. PLoS Pathog. **9:** e1003378.

**Wen, R.H., and Hajimorad, M.R.** (2010). Mutational analysis of the putative pipo of Soybean mosaic virus suggests disruption of PIPO protein impedes movement. Virology **400:** 1–7.

**Wimmer, P., Schreiner, S., and Dobner, T.** (2012). Human pathogens and the host cell sumoylation system. J. Virol. **86:** 642–654.

**Wu, C.Y., Jeng, K.S., and Lai, M.M.** (2011). The SUMOylation of matrix protein M1 modulates the assembly and morphogenesis of Influenza A virus. J. Virol. **85:** 6618–6628.

**Xiong, R., and Wang, A.** (2013). SCE1, the SUMO-conjugating enzyme in plants that interacts with NIb, the RNA-dependent RNA polymerase of Turnip mosaic virus, is required for viral infection. J. Virol. **87:** 4704–4715.

**Xu, K., et al.** (2011). Modification of nonstructural protein 1 of Influenza A virus by SUMO1. J. Virol. **85:** 1086–1098.

**Yoo, S.D., Cho, Y.H., and Sheen, J.** (2007). Arabidopsis mesophyll protoplasts: a versatile cell system for transient gene expression analysis. Nat. Protoc. **2:** 1565–1572.

**Zhang, L., Chen, H., Brandizzi, F., Verchot, J., and Wang, A.** (2015). The UPR branch IRE1-bZIP60 in plants plays an essential role in viral infection and is complementary to the only UPR pathway in yeast. PLoS Genet. **11:** e1005164.

**Zhu, H., Hu, F., Wang, R., Zhou, X., Sze, S.-H., Liou, L.W., Barefoot, A., Dickman, M., and Zhang, X.** (2011). Arabidopsis argonaute10 specifically sequesters miR166/165 to regulate shoot apical meristem development. Cell **145:** 242–256.